A NEXT-TO-LEADING-ORDER CALCULATION OF PROTON-PROTON(PROTON-ANTIPROTON) TO TWO JETS, AT LEAST ONE OF WHICH CONTAINS A CHARM QUARK

BY

WILLIAM J. LINK

DISSERTATION

Submitted in partial fulfillment of the requirements
for the degree of Doctor of Philosophy in Physics
in the Graduate College of the
University of Illinois at Urbana-Champaign, 2012

Urbana, Illinois

Doctoral Committee:

Professor John Stack, Chair
Professor Scott Willenbrock, Director of Research
Professor Brian Fields
Professor Mark Neubauer

Abstract

In this thesis, I present a next-to-leading-order (NLO) calculation for the production of two jets, at least one of which contains a charm quark, which is an important background to single-top production. I discuss the leading order results and their scale dependence before outlining the difficulties of an NLO calculation, and the need for treating the charm quarks as massive in a few areas of the calculation. The NLO corrections turn out to be rather modest, but taking the calculation to NLO greatly improves scale uncertainty.

To my parents Deborah and Steven Link

and to Courtney for being patient

Acknowledgements

First and foremost, I've been lucky in my graduate experience to work with great advisors. So I owe a big thanks to John Campbell, Fabio Maltoni, Tim Stelzer and Scott Willenbrock.

A project like this has its up and its downs, and it would have been absolutely impossible to finish without the help and support of many people. Without Celia Elliot's help navigating university bureaucracy I would probably still be in the graduate fellowship office trying to get applications together. Chris Bonnell provided much needed computing power to finalize a lot of the numbers used in this thesis. Joe Gezo's unwavering dedication to science kept me sane in several low points in my graduate school experience. I owe a debt to Kevin Mantey whose constant stream of interesting electricity and magnetism questions is a good reminder of why I decided to go to graduate school.

Finally, I owe a big thanks to the people who got me out of my head throughout graduate school. Thanks to Rogan Carr, Nick Bronn and David Wells for the weekly physics happy hour. Thanks to James Reed, Meng Liang and the rest of the group for Friday lunches at Dos Reales. Thanks to Nic Salovich for movie and book recommendations. Thanks to Larissa Lorenz, Sean Murray, Maria Ubiali, Lawrence Soung Yee, and Simone Zonnetti for showing me around Brussels. Thanks to all my roommates over the years: Jeff Comer, Joe Yasi, Greg Thompson, Andrew Maginniss, Rosona Eldred,Terra Walston,Yonaton Bisk and Luca Livio for countless dinners, conversations, drinks and diversions.

This work was supported in part by an LHC Theory Initiative Fellowship, NSF grant PHY-0705682 and by US Department of Energy contract No. DE-FG02-91ER40677.

Table of Contents

List of Tables . . . . . **vi**

List of Figures . . . . . **viii**

Chapter 1 Introduction **1**
1.1 Motivation 1
1.2 Renormalization and Scales 2
1.3 QCD and Factorization 6

Chapter 2 The Leading Order Results **11**
2.1 Wcc at Leading Order 11
2.2 Wcj at leading order 13

Chapter 3 The Next-To-Leading-Order Calculation **15**
3.1 Real and Virtual Corrections 15
3.2 Accomplishing divergence cancellation in a Monte Carlo program 17
3.2.1 Building a Dipole 21
3.3 The Need for Massive Quarks 24
3.4 The Processes involved in the NLO calculation 26

Chapter 4 Checks and Results **28**
4.1 Checks 28
4.2 Results 29

Appendix The Massive Loop Matrix Element **38**

References **40**

List of Tables

2.1 Wcc cross sections. The column for process 2 also contains the interference term. A comparison of the process 1 and the more exotic process 2 for W^+,W^- at the LHC and for the Tevatron. Process 1 follows the 2/3 pattern you would expect from Drell-Yan W production at the LHC, and Process 2 doesn't matter much at the Tevatron. All cross-sections in pb . . 12

2.2 Wcj, broken up by initial state. At the LHC (and to a lesser extent the Tevatron), the initial gluons dominate the process. All cross-sections in pb. 13

3.1 All of the processes required for the NLO calculation. q or q' could be charm quarks. For instance $gs- > Wc\bar{q}q$ includes $gs \to Wc\bar{c}c$. For the tree level elements, we use the matrix elements of Nagy and Trocsanyi [1]. For the one loop elements, we use the matrix elements of Bern,Dixon and Kosower [2], with the exception being the massive charm loop where we instead use a finite charm quark mass to regulate the collinear divergence, which can be seen in the appendix. 27

4.1 Exclusive cross sections (pb) for W boson plus tw jets, with at least one c jet, at the Tevatron ($\sqrt{s} = 1.96$ TeV $p\bar{p}$, $p_T > 15$ GeV and $|\eta| < 2$) and LHC ($\sqrt{s} = 14$ TeV pp, $p_T > 25$ GeV and $|\eta| < 2.5$). Two final-state partons are merged into a single jet if $\Delta R_{jj} < 0.7$. No branching ratios or tagging efficiencies are included. The labels on the columns have the following meaning: Wcj = exactly two jets, one of which contains a c quark; $Wc\bar{c}$ = exactly two jets, both of which contain a c quark; $W(c\bar{c})j$ = exactly two jets, one of which contains two c quarks; $W(c\bar{c})c$ = exactly two jets, one of which contains two c quarks, the other a single c quark; $Wcjj$ = exactly three jets, one of which contains a c quark; $Wc\overline{c}j$ = exactly three jets, two of which contain a c quark;$Wccc$ = exactly three jets, all of which are c quarks. For the last set of processes, which include both light and heavy partons in the final state, the labels mean: Wjj = exactly two jets; $Wjjj$ = exactly three jets. For Wcj, $Wc\bar{c}$, and Wjj, both the leading-order (in parentheses) and next-to-leading-order cross sections are given. The CTEQ6M parton distribution functions are used throughout, except for the LO cross sections in parentheses, where CTEQ6L1 is used [3]. The factorization and renormalization scales are chosen as $\mu_F = \mu_R = M_W$. 30

4.2 Inclusive cross sections (pb) for W boson plus two (or more) jets, with at least one c jet, at the Tevatron ($\sqrt{s} = 1.96$ TeV $p\bar{p}$, $p_T > 15$ GeV and $|\eta| < 2$) and LHC ($\sqrt{s} = 14$ TeV pp, $p_T > 25$ GeV and $|\eta| < 2.5$). Two final-state partons are merged into a single jet if $\Delta R_{jj} < 0.7$. No branching ratios or tagging efficiencies are included. The labels on the columns have the following meaning: $Wcj + X$ = two or more jets, one of which contains a c quark; $Wc\bar{c} + X$ = two or more jets, both of which contain a c quark; $W(c\bar{c})j$ = exactly two jets, one of which contains two c quarks; $W(c\bar{c})c$ = exactly two jets, one of which contains two c quarks, the other a single c quark; For the last set of processes, which include both light and heavy partons in the final state, the labels mean: $Wjj + X$ = two or more jets; For $Wcj + X$, $Wc\bar{c} + X$, and $Wjj + X$, both the leading-order (in parentheses) and next-to-leading-order cross sections are given. The CTEQ6M parton distribution functions are used throughout, except for the LO cross sections in parentheses, where CTEQ6L1 is used [3]. The factorization and renormalization scales are chosen as $\mu_F = \mu_R = M_W$. The uncertainties are from the variation of the renormalization scale, the factorization scale, and the parton distribution functions, respectively. 31

List of Figures

1.1 One representative Feynman diagram for $qq' \to Wh$, and one for $qq' \to Wt$ 2
1.2 The standard photon self-energy. 3
1.3 Diagrams for electron-electron scattering as the scale is reduced is reduced relative to the mass of the Z boson 5
1.4 Deep inelastic scattering off of the proton 6
1.5 Parton Model 8
1.6 The left diagram is the leading order diagram for lepton scattering off a parton, which determines a pdf for the parton q. The right diagram is an NLO correction to this pdf due to the presence of gluons in the proton 9

2.1 The diagrams for Wcc. I refer to the left diagram as process 1, and the right diagram as process 2 in the table below. 12
2.2 The leading-order diagram for Drell-Yan production. Protons have more valence u quarks than ds, so W^+ is favored in pp collisions 12
2.3 The leading order processes for Wcj. 13
2.4 Scale Uncertainties at the Tevatron. The renormalization and factorization scales are being varied from $\frac{M_W}{2}$ to $2M_W$. 14
2.5 Scale Uncertainties for W^+ production at the LHC. The renormalization and factorization scales are being varied from $\frac{M_W}{2}$ to $2M_W$. 14

3.1 The left diagram shows an NLO correction due to an initial gluon. The right diagram focuses on the gluon leading to the correction 15
3.2 The left diagram is the leading order diagram for lepton scattering off a parton, which determines a pdf for the parton q. The right diagram is an NLO correction to this pdf due to the presence of gluons in the proton 16
3.3 An example correction due to real gluon emission on the left. On the right, a close up of the quark line emitting the gluon 16
3.4 A correction due to virtual gluons. The diagram on the right shows the correction to the boson/quark vertex due to gluons. This corrects both parton distribution functions and our process 17
3.5 Dipole Factorization diagrammatically. In the collinear limit, the matrix element factorizes to the leading order multiplied by a dipole piece associated with collinear/soft divergences . . 20
3.6 Two diagrams involved in $Wccc$ production 24
3.7 Two diagrams involved in $Wccj$ production 24
3.8 To maintain gauge invariance, the charm line at the top of both diagrams must be handled massively 25
3.9 This virtual charm quark loop must be handled with non-zero mass or it has an uncanceled final state divergence. 26

4.1 Scale dependence for Wcc and Wcj at LO and for inclusive NLO production at the Tevatron. The dashed line is NLO. 29

4.2 Scale dependence for Wcc and Wcj at LO and for inclusive NLO production at the LHC. The dashed line is NLO 30
4.3 Exclusive cross section for Wcj and Wcc at NLO at the Tevatron vs the p_t of the highest jet. The dashed lines are the processes for $W(cc)j$ and $W(cc)c$. The lower plot contains the ratio of the NLO to LO cross sections. All parameters as described for TeV in table 4.1 32
4.4 Same as figure 4.3 but for the p_t of the lepton from W decay 33
4.5 Same as figure 4.3 but for the dijet invariant mass 34
4.6 Exclusive cross section for Wcj and Wcc at NLO at the LHC vs the p_t of the highest jet. The dashed lines are the processes for $W(cc)j$ and $W(cc)c$. The lower plot contains the ratio of the NLO to LO cross sections. All parameters as described for LHC in table 4.1 35
4.7 Same as figure 4.6 but for the p_t of the lepton from W decay 36
4.8 Same as figure 4.6 but for the dijet invariant mass 37

Chapter 1

Introduction

This chapter introduces the motivation for this background calculation, and gives a very brief overview of the source of renormalization and factorization scale dependence in QCD calculations.

1.1 Motivation

The main motivation for looking at a calculation of $pp\,(p\bar{p}) \to W+$ 2 jets, one of which contains a charm jet (Wcc for two charm production, Wcj for one charm) is that it is an important background for a number of important standard model processes, in particular Higgs production and single top.

While the experimental discovery of the Z boson at CERN confirmed a great deal Weinberg, Salam, and Glashow's electroweak theory, and propelled the trio to the Nobel Prize, the scalar particle predicted by their theory has yet to be confirmed. The desire to confirm the Higgs has even been picked up by popular media, with the recent announcements from the LHC being reported as headline news.

While the Higgs is the only standard model particle yet to be confirmed, there are further important processes experimentalists would like to observe and which may lead to physics beyond the standard model. One such process is single top production, which is an interesting process for several reasons. First, its sensitive to the couplings between the top and bottom quarks V_{tb} [4, 5]. It is also directly sensitive to the b quark distribution function [6], which also has yet to be measured directly.

Figure 1 shows representative Feynman diagrams for both Higgs and single top production that are relevant at both the LHC and Fermilab's Tevatron. The W in the final state is nice experimentally as the W can decay leptonically, which makes a nice clean experimental signal. The two heavy quarks are difficult to detect experimentally, but unfortunately a hallmark of both single top and Higgs processes. The Higgs, which is responsible for providing mass to the particles of the standard model, couples most strongly to heavier objects. Hence, it is most likely to decay to heavier objects. Bottom quarks are also unavoidable in single top signals, as the very heavy top quark will decay quite quickly to a bottom quark.

In order to detect either of these signals, experimentalists need to separate the needle of the signal from

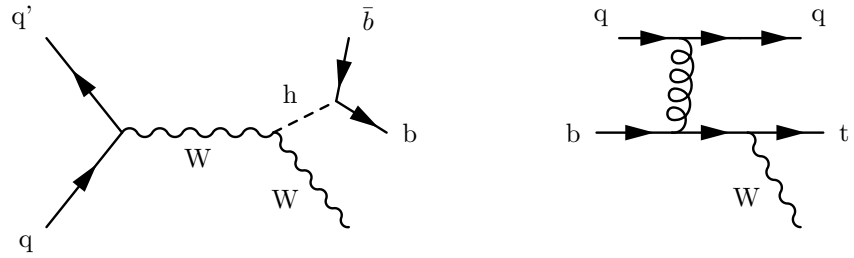

Figure 1.1: One representative Feynman diagram for $qq' \to Wh$, and one for $qq' \to Wt$

the haystack that is all of the other processes that produce a W boson and heavy quarks [7–10]. Thus, its very important to characterize as best as possible the standard model backgrounds involving W bosons and heavy quarks. For these reasons, a next to leading order calculation has recently been done for production of W and two jets one or more of which contains a b quark [6].

However, this calculation isn't enough. The way experimentalists determine whether a jet contains a heavy quark is by looking for secondary vertices, because heavy quarks travel away from the primary vertex before the decay. This decay law is exponential, and depends on the mass. What this means is that charm quarks occasionally "fake" bottom quarks. To understand the background, a calculation of Wcjet needs to be done.

1.2 Renormalization and Scales

The story of next-to-leading-order calculations in QCD, like all stories in field theory, involves a lot of technical details, and I want to instead start the story with QED, which is defined as a theory with a $U(1)$ symmetry, with one massive fermion.

$$\mathcal{L} = i\bar{\psi}\gamma^\mu\partial_\mu\psi + g\bar{\psi}\gamma^\mu A_\mu\psi - m\bar{\psi}\psi - \frac{1}{4}F^{\mu\nu}F_{\mu\nu} \tag{1.1}$$

Amazingly, this Lagrangian, and the rules developed to quantize these things, contains Maxwell's equations and Dirac's equation.

But viewing this theory in terms of its $U(1)$ symmetry and particle content leads to an interesting question about the Lagrangian. Why is it truncated after only a few terms that respect the symmetry? Why not have terms such as $\bar{\psi}\psi\bar{\psi}\psi$? After all, this term has the same gauge symmetry. There is also one other problem, as I'll demonstrate below, certain calculations in the theory appear divergent. Surprisingly enough both of these issues are addressed with the same physical insight.

The physical insight is that we should expect that our theory is fundamentally a theory of long length scale, as thats where our measurements have taken place. Long wavelength physics should be relatively

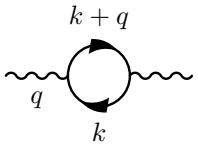

Figure 1.2: The standard photon self-energy.

insensitive to the exact form of short wavelength interactions.

To emphasize that our theory is only valid at some long distance scale, we rewrite our Lagrangian as

$$\mathcal{L} = i\bar{\psi}\gamma^\mu\partial_\mu\psi + g_r\bar{\psi}\gamma^\mu A_\mu\psi - m_r\bar{\psi}\psi - \frac{1}{4}F^{\mu\nu}F_{\mu\nu} + \delta_2 i\bar{\psi}\gamma^\mu\partial_\mu\psi + g_r\delta_1\bar{\psi}\gamma^\mu A_\mu\psi - \delta_m\bar{\psi}\psi - \delta_3\frac{1}{4}F^{\mu\nu}F_{\mu\nu} \quad (1.2)$$

The parameters g and m are measured at some known scale, and thus contain coarse-grained contributions from lots of high energy degrees of freedom. The δ counter terms are needed in perturbative calculations to keep us from over-counting contributions from the high energy degrees of freedom, as those contributions are already contained in the measured parameters.

To see this, lets consider the standard photon self energy, seen in diagram 1.2.

Evaluating the leading order term in the loop integral[1]

$$i\Pi^{\mu\nu}\left(q^2\right) \propto \int d^4k \frac{k^2}{\left(k^2-m^2\right)\left((k+q)^2-m^2\right)} \quad (1.3)$$

We see that this is divergent, but that divergence comes from the high energy degrees of freedom. However, our rather course-grained measurement of g_r should already contain these high energy contributions. Hence, we need to include the counter term δ_3, to subtract off the contribution from the high energy physics. Handling the calculation in dimensional regularization, we find

$$i\Pi^{\mu\nu}\left(q^2\right) = \left(q^2\eta^{\mu\nu} - q^\mu q^\nu\right) i\Pi\left(q^2\right) \quad (1.4)$$

$$i\Pi\left(q^2\right) = -\frac{2\alpha}{\pi}\int_0^1 dx x\left(1-x\right)\left(\frac{2}{\epsilon} - \log\Delta - \gamma + \log\left(4\pi\right)\right) + \delta_3 \quad (1.5)$$

[1]This section owes much to material in Peskin [11]

where

$$\Delta = m^2 - x(1-x)q^2 \tag{1.6}$$

In the above, ϵ is approaching 0, so the first term parameterizes our divergence. γ is the Euler-Mascheroni constant. Next, we need a way to decide on the counter term. Clearly, δ_3 will cancel the divergence, which obviously comes from the short length scale physics, but we need a way to decide what short-wavelength physics is already included in our coupling constants. Such a prescription is a renormalization condition. For now, we choose

$$\Pi\left(\mu_r^2\right) = 0 \tag{1.7}$$

μ_r is known as a renormalization scale. Choosing an appropriate μ_r, this gives us

$$\Pi\left(q^2\right) = \frac{2\alpha}{\pi}\int_0^1 dx x\left(1-x\right)\log\frac{m^2-\left(1-x\right)q^2}{m^2-\left(1-x\right)\mu_r^2} \tag{1.8}$$

So, we can see how restricting our theory to an appropriate length scale has regulated our divergence. But, we still need to see how this solves the problem of the number of terms to hold in our Lagrangian. To see this, imagine following the standard technique for summing up the diagrams for the photon self energy.

$$-i\frac{q^2}{1-\Pi\left(q^2\right)}g^2 \tag{1.9}$$

Now, we note that in the specific case of the photon, every propagator has a charge g associated with each end, so we can think of the photon self-energy as being intimately related to the value of the charge. In particular, we can interpret

$$g\left(q^2\right) = g_r\sqrt{\frac{1}{1-\Pi\left(q^2\right)}} \tag{1.10}$$

This implies that the value of g we measure has an implicit dependence on μ_r, the scale where we make our measurements. We can deduce from this how g will change if we choose a different scale for our renormalization

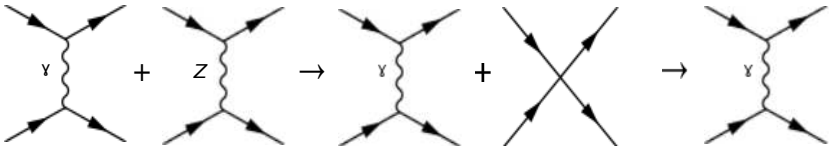

Figure 1.3: Diagrams for electron-electron scattering as the scale is reduced is reduced relative to the mass of the Z boson

$$\beta = \mu_r \frac{\partial g}{\partial \mu_r} = g\frac{2\alpha}{\pi}\frac{1}{6} = g\frac{e^2}{12\pi^2} \tag{1.11}$$

In the above, I took m to 0, which assumes we are working at a scale much higher than the mass of the electron.

Now, this equation, the β function, is extremely important. What this equation[2] does is define a family of effective theories, each describing the same physics at different length scales. Now, we can return to our original Lagrangian, with all of the extra higher order terms, and ask what happens as we decrease the renormalization scale?

Ken Wilson [12] won the Nobel Prize for discovering that higher order operators will run to 0 as the scale increases. I won't reproduce the full technical details here, but I will give a plausibility argument. Essentially, what renormalization tells us is that for long-length-scale effective theories, higher order operators become irrelevant. Why might that be? All terms in a 4d lagrangian have a mass dimension of 4, so that the path integral comes out unitless. Consider the operator $\bar{\psi}\psi\bar{\psi}\psi$. Each field ψ has a dimension of $m^{\frac{3}{2}}$, so the total dimension of the operator is 6. This means the operator must have a coefficient g which has a mass dimension of m^{-2}, we can represent this has $g \propto \frac{\hat{g}}{\Lambda^2}$. Going to longer length scales is equivalent to running that scale Λ higher and higher, which diminishes the strength of the operator.

This understanding of renormalization has many advantages. In particular, if we ever find that perturbation theory is failing to converge, we can use a theory at a different scale where convergence is better. Unfortunately, these advantages come at a cost. The scale we use μ_r will find its way into any calculation we perform. While full perturbative calculations must be completely scale invariant, each order will still have scale dependence (if this weren't true, changing scale would never improve convergence). This scale dependence can lead to very large uncertainty, particularly in leading order calculations.

And in QCD, as we will soon see, we will have to introduce another scale into our calculations.

[2]Along with a similar equation for the mass of electron

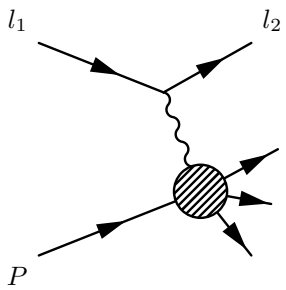

Figure 1.4: Deep inelastic scattering off of the proton

1.3 QCD and Factorization

First, lets take a minute to motivate QCD.[3] Consider a process as shown in the figure. A high energy electron scatters off of a proton, which blows apart into a variety of hadrons.

To begin our analysis, we will assume the scale is such that the mass of the electron is unimportant. And it is always useful to define Lorentz invariant quantities. Using k for the momenta of the photon, p for the momenta of the leptons, and P the momenta of the proton.

$$Q^2 = -k^2 \tag{1.12}$$

$$\nu = \frac{P \cdot k}{M} \tag{1.13}$$

Now, QED tells us how to deal with the amplitude associated with the electron emitting the photon in the diagram above. But how can we deal with the photons interaction with the proton? We use one of the insights from QED- photons couple to conserved currents. We can represent this current $\langle X| J^\mu |P\rangle$. This is the hadronic current. Note, it is conserved, i.e. $k_\mu \langle X| J^\mu |P\rangle = 0$.

We can now follow the standard Feynman rules to write the amplitude squared associated with this diagrams

$$|\mathcal{M}|^2 = \frac{1}{4}\sum_{spins} |\mathcal{M}|^2 = \frac{e^4}{Q^4}\left(2p_1^\mu p_2^\nu + 2p_1^\nu p_2^\mu - 2\eta^{\mu\nu} p_1 \cdot p_2\right)\left(\frac{1}{2}\langle P| J^\mu |X\rangle \langle X| J_\nu |P\rangle\right) \tag{1.14}$$

The first term in parentheses can be associated with the scattering of the electron. We can refer to it as $L^{\mu\nu}$ from now on. The second term is associated with the hadronic current. The standard formula for the cross section tells us

[3]This section follows Scott Willenbrock's lecture notes on NLO Drell-Yan [13]

$$d\sigma = \frac{1}{2\left(S-M^2\right)}\left|\mathcal{M}\right|^2 \frac{d^3p_2}{\left(2\pi\right)^3 2E_2} dX \left(2\pi\right)^4 \delta^4\left(P+k-X\right) \tag{1.15}$$

The goal here is to lump everything depending on hadronization into one term, so we'll pull the integral over the phase space of the hadrons, dX, and the delta function involving the hadrons momenta into one term.

$$W_{\mu\nu} = \frac{1}{2}\frac{1}{4\pi M}\int dX \left\langle P\right| J_\mu \left|X\right\rangle \left\langle X\right| J_\nu \left|P\right\rangle \left(2\pi\right)^4 \delta^4\left(P+k-X\right) \tag{1.16}$$

So the total cross section is

$$d\sigma = \frac{4\pi M}{2\left(S-M^2\right)}\frac{e^4}{Q^4} L^{\mu\nu} W_{\mu\nu} \frac{d^3p_2}{\left(2\pi\right)^3 2E_2} \tag{1.17}$$

Now, it seems like we don't know anything at all about the W tensor. However, we can invoke both the power of conservation $k^\mu W_{\mu\nu} = 0$, the fact that QED conserves parity, and Lorentz invariance to note that W will have the form

$$W_{\mu\nu} = -\frac{1}{2M}\left(\eta_{\mu\nu} + \frac{k_\mu k_\nu}{Q^2}\right) F_1\left(x, Q^2\right) + \frac{1}{M^2\nu}\left(P_\mu + k_\mu \frac{P\cdot k}{Q^2}\right)\left(P_\nu + k_\nu \frac{P\cdot k}{Q^2}\right) F_2\left(x, Q^2\right) \tag{1.18}$$

F_1 and F_2 are dimensionless, and known as the form factors. We are now in a position that I can report the mystery[4] of deep inelastic scattering. It was discovered at SLAC that at high Q^2 instead of depending on the two independent variables, Q and ν, the form factors depended only on the ratio, $x = \frac{Q^2}{2M\nu}$. How can we think about this strange fact?

Feynman [14] gave us the answer. Imagine that instead of scattering off the proton, the virtual photon scatters instead off of a massless quark, only weakly bound to its neighbors. The quark will carry some fraction of the momentum of the proton, which I've called y in the figure. Assuming Q^2 is much larger than the mass of the final quark, then we find

$$(p_1+k)^2 = 0 = 2yP\cdot k - Q^2 \implies y = \frac{Q^2}{2P\cdot k} = x \tag{1.19}$$

We see that it is natural that the form factors depend on x. We can represent x as the fraction of the protons momenta carried by the quark. We also see that its natural that the form factor doesn't depend on Q^2. Without M, the mass of the proton, there is no other massless ratio we can make with Q^2.

[4]Its less of a mystery than I'm making it out to be. Bjorken predicted this mystery before any measurement was made

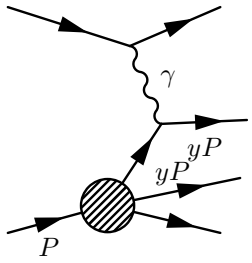

Figure 1.5: Parton Model

Like any good answer, this leads to more questions. This argument relies on weakly bound quarks, but obviously protons are bound strongly enough to overcome Coulomb repulsion. We need a theory that allows for a quark to be weakly bound at high energy, but strongly bound at high energies. The answer is QCD.

$$\mathcal{L}_{QCD} = i\bar{\psi}_i \left(i\gamma^\mu \partial_\mu - m\right) \psi_i - g G^a_\mu \bar{\psi}_i \gamma^\mu T^a_{ij} \psi_j - \frac{1}{4} G^a_{\mu\nu} G^{\mu\nu}_a \tag{1.20}$$

If we calculate the β function for QCD to leading order, we find

$$\beta\left(\alpha_s\right) = \frac{\partial \alpha_s}{\partial \ln Q^2} = -\alpha_s^2 \frac{1}{12\pi} \left(33 - 2n_f\right) \tag{1.21}$$

If $n_f < 17$, we see that this has the opposite sign of QED. As we go to longer length scales, the coupling grows stronger. In particular, at some value of the scale [15] $\Lambda_{\text{QCD}} \approx 200\text{MeV}$, perturbation theory will break down completely.

This leads to a conundrum when doing calculations. Standard quantum field theory techniques for calculation cross-sections are built by expanding on states that are free in the infinite past and infinite future. In QCD, however, neither the quarks nor the gluons are good degrees of freedom far in the past or future, protons and neutrons are. [5] This problem shows up as infrared divergences in diagrammatic calculations.

To see the solution to this problem, lets press onward with our description of deep inelastic scattering. We need to define for the proton parton distribution functions $f_i\left(y\right)$. These describe the probability of finding a parton, i, with momentum fraction y of the proton's four momenta. In this notation, we note that the differential cross section can be written

$$d\sigma = \sum_i \int_x^1 dy f_i\left(y\right) d\hat{\sigma}_i \tag{1.22}$$

[5] This problem is not actually unique to QCD. We have the same problem in QED- the electron isn't a good state, which shows up in infrared divergences. The good state is an electron and a cloud of soft real photons [11]

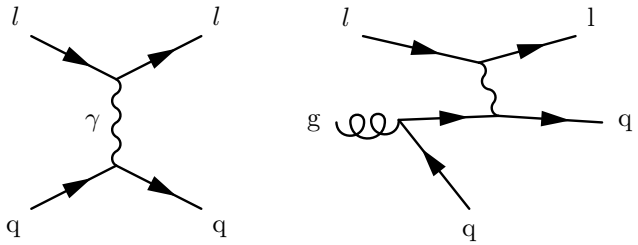

Figure 1.6: The left diagram is the leading order diagram for lepton scattering off a parton, which determines a pdf for the parton q. The right diagram is an NLO correction to this pdf due to the presence of gluons in the proton

Here, $d\hat{\sigma}_i$ is the differential cross section for each parton sub-process. We can calculate the subprocess seen on the diagram. If we use

$$W_{\mu\nu} = \frac{1}{4\pi M} \sum_i \int_x^1 \frac{dy}{y} f_i(y) \hat{W}^i_{\mu\nu} \tag{1.23}$$

we evaluate the diagram to find

$$\hat{W}^i_{\mu\nu} = 2q_i^2 \left(2y^2 P_{\mu\nu} + yq_\mu P_\nu + yq_\nu P_\mu - y\eta_{\mu\nu} P \cdot q\right) 2\pi \frac{\delta(y-x)}{2P \cdot q} \tag{1.24}$$

Using 1.23 and 1.18, we find

$$F_1\left(x, Q^2\right) = \sum_i q_i^2 f_i(x) \tag{1.25}$$

$$F_2\left(x, Q^2\right) = \sum_i q_i^2 x f_i(x) \tag{1.26}$$

This is all well and good, but lets look at what happens at higher order in perturbation theory.

At higher order in perturbation theory, our pdf is actually divergent! To see this, consider the propagator of the gluon in the right diagram.

$$S \propto \frac{1}{\left(p_1 + p_2\right)^2 - m^2} = \frac{1}{2p_1 \cdot p_2} \tag{1.27}$$

Here, p_1 and p_2 are the four momenta of the quark and gluon respectively. I've also used the general fact that for a four momentum p, $p^2 = m^2$.

If we choose the original gluon to be moving along z, we can parameterize the gluon and quark momenta as follows

$$p_1 = (E_1, 0, 0, E_1) \tag{1.28}$$

$$p_2 = (E_2, 0, E_2 \sin(\theta), E_2 \cos(\theta)) \tag{1.29}$$

$$p_1 \cdot p_2 = E_1 E_2 (1 - \cos\theta) \tag{1.30}$$

$$\implies S \propto \frac{1}{2E_1 E_2 (1 - \cos\theta)} \tag{1.31}$$

Here, θ is the angle between p_1 and p_2. From this expression we can begin to see the divergences associated with this type of real gluon correction. As $\theta \to 0$, the propagator blows up, and we have a collinear divergence. This divergent area of phase space cannot be avoided, since our quark's momenta is proportional to the proton's. We can parameterize this divergence as

$$\alpha_s \ln\left(\frac{\Lambda^2}{Q^2}\right) \tag{1.32}$$

where Λ is an arbitrary scale. The divergence is in the limit of small Λ, and just like in renormalization, it underscores a need to recognize that our measurements of the quark pdfs, f_i, were done at one scale. We can define a parton distributions at one scale. From here on out, we'll call this scale μ_f, the factorization scale.

Just like with renormalization, introducing this scale will create an implicit scale dependance in the parton distribution functions. The analogy of the β function is the DGLAP equation [15]. Using f_q for quark distribution functions, and f_g for gluons, we can write the contribution to the quark function evolution coming from initial gluons as

$$\frac{d}{d\ln Q^2} f_q(x, Q^2) = \frac{\alpha_s}{2\pi} \int_x^1 \frac{dy}{y} f_g(y, Q^2) P_{qg}\left(\frac{x}{y}\right) \tag{1.33}$$

Here the P_{qg} are called Altarelli Parisi kernels, and there is one for each type of parton splitting ($q \to g$,$g \to q$,$g \to g$,$q \to q$).

Just like with renormalization, we can use the DGLAP equation to evolve the parton distribution functions to help perturbation theory converge. Unfortunately, just like with renormalization we have to introduce an unphysical scale μ_f, which further increases the scale uncertainty.

Chapter 2

The Leading Order Results

Taken together, we can think of the introductory chapter as a template for doing perturbative QCD calculations. We use the β function and DGLAP equation to evolve the parton distributions and $\alpha(s)$ to a scale suitable for the calculation. For the calculation at hand, we chose $\mu_f = \mu_r = M_W$ where M_W is the mass of the W boson, as its the obvious mass scale of the problem.

Next, these partons go through scattering events as described by Feynman diagram calculations. This short range physics is well described by perturbation theory, as the energy scale of these interactions is well into the region where the strength of the coupling is weak enough to be described by perturbation theory.

Finally, the final state partons must be "hadronized." Bare partons will pull other partons from the vacuum in order to form bound states. This physics is also non-perturbative.

With a few subtleties, this procedure also lends itself nicely to doing monte carlo event simulations. We start with an analytical calculation of a cross section described by perurbative QCD. We then generate an event by using an experimentally measured parton distribution function to generate incoming partons, and conservation of four momentum to generate outgoing partons. This event is weighted by the value of the analytical cross section, and then a new event generated.

For this calculation, I implemented the calculation in MCFM [16], a monte-carlo program originally written by John Campbell and Keith Ellis.

Before turning to the more complicated next-to-leading order process, its important to get our bearings by thoroughly understanding the leading order results. At leading order, we can separate the calculation into two final states, Wcc and Wcj. I'll start the discussion with Wcc.

2.1 Wcc at Leading Order

Process 1 in figure 2.1 is identical to the process previously calculated for b quark production [6]. At the LHC, we can understand the relative importance of W^+ and W^- from Drell-Yan production, shown in figure 2.1. Because of the larger presence of u quarks in the proton, Drell-Yan W^- production is roughly $\frac{2}{3}$ of the

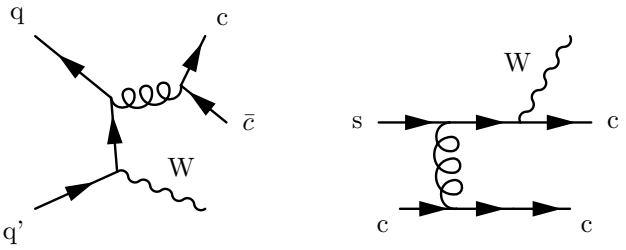

Figure 2.1: The diagrams for Wcc. I refer to the left diagram as process 1, and the right diagram as process 2 in the table below.

more favored W^+ production in pp collision [15].

Process 2 is more exotic. If we allow off-diagonal CKM, process 2 can be sensitive to the d and $\bar{d}$ distribution functions of the proton. Since protons have a valence d content, process 2 will see W^- favored over W^+ in pp collisions.

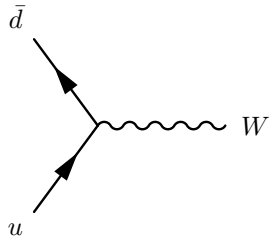

Figure 2.2: The leading-order diagram for Drell-Yan production. Protons have more valence u quarks than ds, so W^+ is favored in pp collisions

With that in mind, lets look at the cross-sections. In the tables below all the leading order processes were run using CTEQ6L1 [3]. For the Tevatron, we run with cuts $\sqrt{s} = 1.96$ TeV,$p_t > 15$ GeV, $\eta < 2.0$,$R > 0.7$. For the LHC we use $\sqrt{s} = 14$ TeV,$p_t > 25$GeV, $\eta < 2.0, R > 0.7$. In all cases, the produced W boson is taken to be on shell. MCFM is more flexible, and does allow the decay of the W boson.

Collider	Process 1	Process 2	Total
W^+ LHC	9.44	7.92	17.36
W^- LHC	6.54	8.98	15.52
TeV ($W^+ = W^-$)	2.46	0.10	2.56

Table 2.1: Wcc cross sections. The column for process 2 also contains the interference term. A comparison of the process 1 and the more exotic process 2 for W^+,W^- at the LHC and for the Tevatron. Process 1 follows the 2/3 pattern you would expect from Drell-Yan W production at the LHC, and Process 2 doesn't matter much at the Tevatron. All cross-sections in pb

Notice that at the Tevatron, the more exotic process is basically unimportant. This is because the sea-quark distributions are relatively unimportant. At the LHC, however, the pdfs for both the gluons and the sea-quarks are much larger. Further, we can see from the process 2 column that the off-diagonal CKM contribution (which can estimate from the difference between W^+ and W^- at the LHC in process 2) is relatively important.

2.2 Wcj at leading order

Wcj is a bit more complicated than Wcc production, as we can see by the number of diagrams.

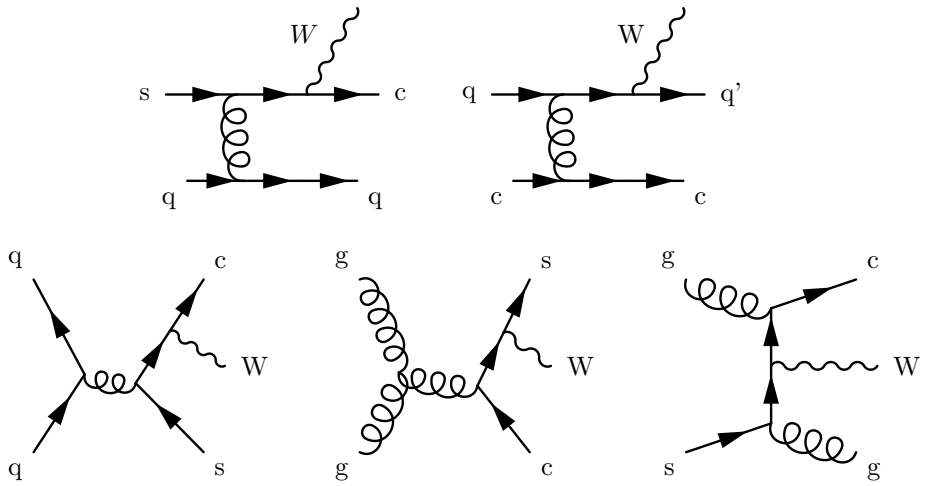

Figure 2.3: The leading order processes for Wcj.

This processes is much more complicated than the equivalent process with b quarks. For Wbj the only diagram is the second. In order to understand the numbers, we'll break the process up into its initial states. As before, we notice that the first two diagrams, and the last diagram are potentially sensitive to the valence quark distributions of the proton. The first and last diagram will tend to favor W^-, through an off-diagonal CKM contribution from the down quark. The second diagram will favor W^+. For this reason, we separate table q into different initial states. The parameters for this table are the same as the one above.

Collider	gq	gg	qq initial charm	qq no initial charm	Total
W^+ LHC	417	122	72	61	672
W^- LHC	459	122	46	68	695
TeV($W^+ = W^-$)	9.43	1.98	1.91	2.49	15.8

Table 2.2: Wcj, broken up by initial state. At the LHC (and to a lesser extent the Tevatron), the initial gluons dominate the process. All cross-sections in pb.

Notice that for the initial charm states, W^+ and W^- at the LHC follow our expected $\frac{2}{3}$ rule of thumb. The gq and no-initial charm states show a slight enhancement in W^- from the off-diagonal CKM couplings, exactly as expected.

These results have fairly large scale uncertainties, as can be seen in the plots in figure 2.4 and 2.5.

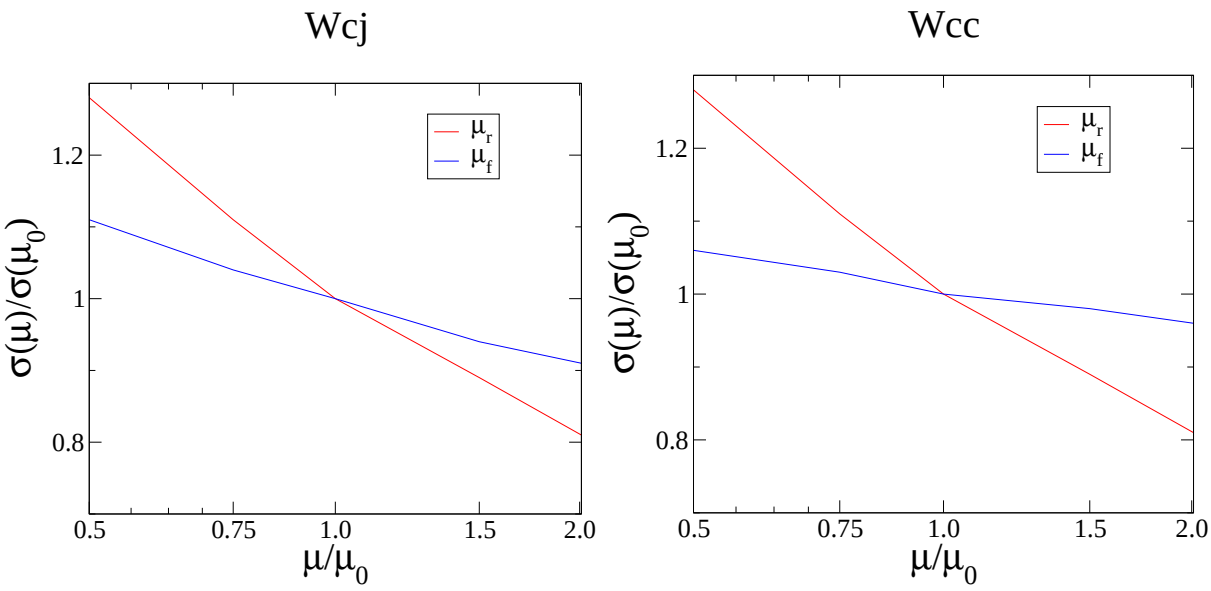

Figure 2.4: Scale Uncertainties at the Tevatron. The renormalization and factorization scales are being varied from $\frac{M_W}{2}$ to $2M_W$.

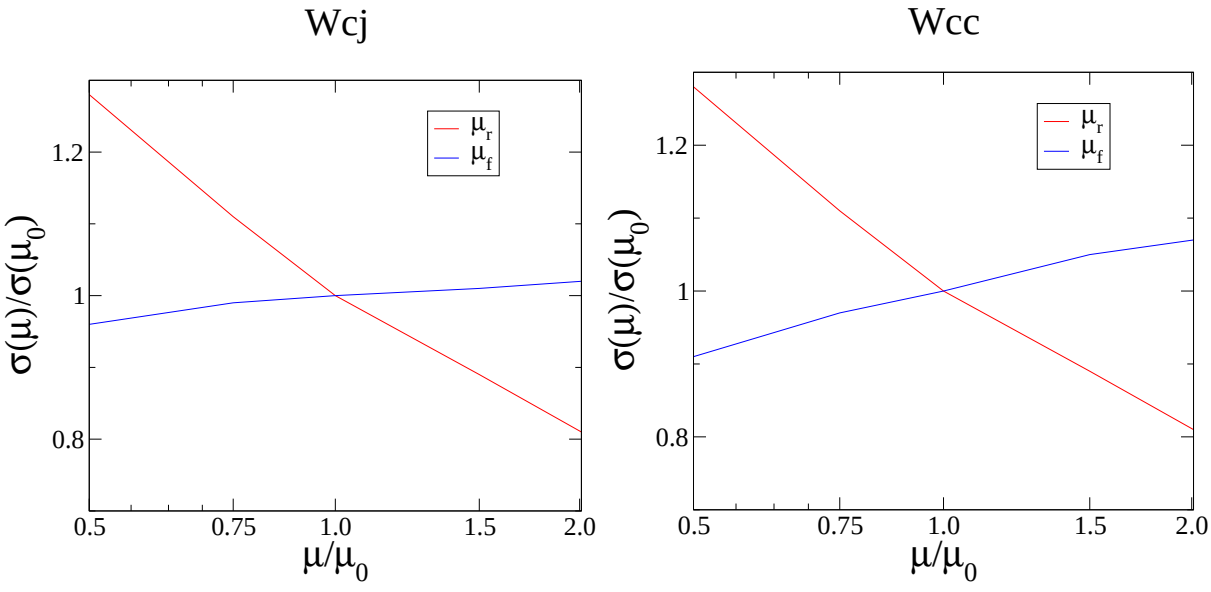

Figure 2.5: Scale Uncertainties for W^+ production at the LHC. The renormalization and factorization scales are being varied from $\frac{M_W}{2}$ to $2M_W$.

Chapter 3

The Next-To-Leading-Order Calculation

This chapter will introduce the technical details required of an NLO calculation, including the types of divergences encountered and how to implement them in a monte-carlo calculation.

3.1 Real and Virtual Corrections

Corrections to the leading order process can be broadly broken in to two categories: corrections due to real gluons, and collections due to virtual loops. We'll start with the corrections from real gluons.

We can either put these extra gluons in the initial or the final state. The diagrams in figure 3.1 demonstrate placing the gluons in the initial state. This gluon then splits into two partons, one of which continues at low transverse momentum and is undetected, the other ends up entering into the leading order process.

The right diagram looks a lot like the correction to the quark pdf we saw in the previous chapter, in particular we note that we expect a divergence when p_1 and p_2 go collinear. The divergence will be parameterized by

$$\ln \frac{\Lambda^2}{M_W^2} \tag{3.1}$$

How can we deal with this collinear divergence? After all, if QCD is a reasonable theory, it should not predict that anything observable is divergent. QCD is a reasonable theory, and there are theorems that tell us that well defined observables will indeed be divergence free [17–19]. The problem is that this single form of NLO correction turns out not be a well defined observable. We have to combine this with another NLO

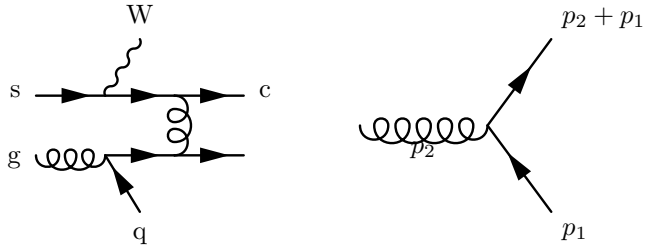

Figure 3.1: The left diagram shows an NLO correction due to an initial gluon. The right diagram focuses on the gluon leading to the correction

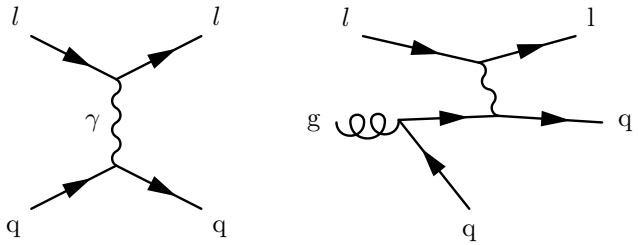

Figure 3.2: The left diagram is the leading order diagram for lepton scattering off a parton, which determines a pdf for the parton q. The right diagram is an NLO correction to this pdf due to the presence of gluons in the proton

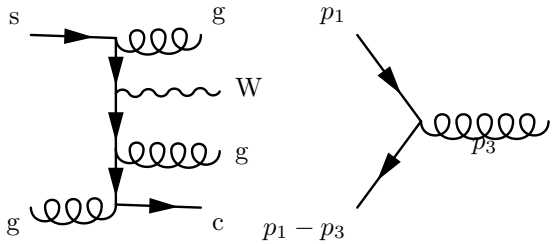

Figure 3.3: An example correction due to real gluon emission on the left. On the right, a close up of the quark line emitting the gluon

correction term.

In order to make an observable that is "infrared-safe" i.e. free of collinear or soft divergences, we have to realize that corrections from real gluons in the initial state are intimately related to corrections to the parton distribution functions. Combining the divergence from initial gluons with the corrections to the distribution functions seen in equation, we see that we expect the Λ dependence drops out.

$$\ln \frac{\mu_f}{M_W} \tag{3.2}$$

The next round of NLO corrections associated with real gluons can be seen in figure 3.3. This is associated with a real gluon in the final state. Notice that the diagram associated with the emission of the gluon is essentially the same diagram as for the gluon splitting seen in the above correction, only now its on its side. For this reason, the collinear divergences mentioned above will appear again.

There is another divergence, now that we have an external gluon line. When the energy of the external gluon gets very small, the quark propagator becomes divergent. We didn't have this divergence before, because the gluon was in the initial state,and we didn't have to integrate over its momentum. With a final state gluon, we will integrate over its possible trajectories, and so we will explore the divergent region of the phase space.

The infrared divergences must find a place to cancel, and for that we turn to the NLO loop diagrams,corrections due to virtual gluons shown in figure 3.4. The infrared behavior of the loop will be dominated by the divergence associated with gluon emission from the quark line. Hence, the infrared di-

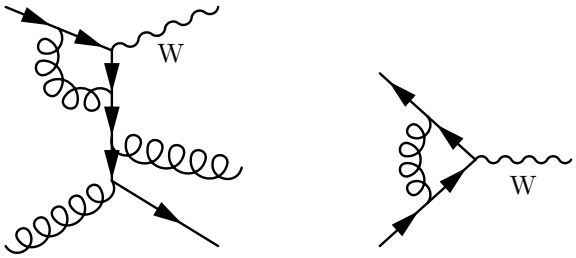

Figure 3.4: A correction due to virtual gluons. The diagram on the right shows the correction to the boson/quark vertex due to gluons. This corrects both parton distribution functions and our process

vergence structure of these loop diagrams will cancel against the infrared divergences associated with real gluon emission. However, these loop diagrams contain collinear singularities with initial state partons that will fail to cancel the collinear singularities associated with the real gluon emission.

To cancel this last set of collinear singularities, we have to once more turn to corrections to parton distribution functions. The collinear corrections due to virtual gluon corrections due to parton distribution functions will exactly cancel the collinear divergences associated with the corrections to the matrix element.

3.2 Accomplishing divergence cancellation in a Monte Carlo program

While all of the divergences associated with the NLO correction will cancel, the structure of this cancellation is fairly inconvenient for monte-carlo implementation. The reason is that various corrections have a different phase space structure associated with them. The corrections due to real emission have four particles in the final state that need to be integrated over, while the corrections due to virtual gluons and the corrections associated with the parton distribution functions have only three particles in the final state.

This means that we cannot directly combine the corrections before integrating them, and since we are doing the integrations by monte carlo event generation, we need some way to manage the divergences.

MCFM deals with this problem using the dipole method of Catani and Seymour.[1] The approach is simple. We create counter-terms that exactly approach the real matrix elements in the soft and collinear regions, which we subtract from the real matrix elements. These counter-terms are known as dipole terms. This makes the real matrix element finite throughout phase space, and so we can directly integrate it.

[1]This section is a summary of Catani and Seymour [20]

$$\sigma_{NLO} = \int_{m+1} (d\sigma_{Real} - d\sigma_{Dipole}) + \int_{m+1} d\sigma_{Dipole} + \int_{m} d\sigma_{Virtual} \tag{3.3}$$

$$= \int_{m+1} (d\sigma_{Real} - d\sigma_{Dipole}) + \int_{m} \left(d\sigma_{Virtual} + \int_{1} d\sigma_{Dipole} \right) \tag{3.4}$$

We further structure the dipole terms so that they factor nicely and one particle degree of freedom can be integrated out. After integrating out this degree of freedom, we can then add back what we've taken out of the real element into the virtual element. This should make the virtual matrix element finite, so we can then integrate directly over it. Having outline this calculation, lets proceed to discuss building these dipoles.

The dipole content is motivated by the fact that the behavior of a matrix element as it emits a gluon that goes soft or collinear is universal. Consider, for instance the gluon emission diagram shown in figure x. If we parameterize the soft divergence by taking the gluon momentum to be λq, for some small λ,we can write the part of the Feynman diagram[2] created by adding the gluon is (to order $\frac{1}{\lambda}$)

$$\frac{(\not{p} + \lambda \not{q} + m) \gamma^{\mu} u(p) \epsilon_{\mu}}{(p + \lambda q)^2 - m^2} \tag{3.5}$$

Here p is the four momentum of emitting quark, and epsilon is the polarization vector of the gluon, and I have used feynman slash notation. γ are the gamma matrices that show up whenever we have fermions. $u(p)$ is the momentum space wavefunction of the emitting quark. Using the clifford algebra for the gamma matrices we can simplify the numerator (retaining only leading order in λ)

$$(2p^{\mu} - \gamma^{\mu} \not{p} + \gamma^{\mu} m) \epsilon_{\mu} u(p) \tag{3.6}$$

We recognize the second two terms as the dirac equation, which $u(p)$ satisfies, so

$$(2p^{\mu} \epsilon_{\mu}) = 2p \cdot \epsilon \tag{3.7}$$

We can combine this with the denominator to get

[2]Actually, I've ignored a color factor associated with the emission of the gluon. It leads to a factor of $\langle c_1, ..., c_m | T_{ij} \cdot T_k | a_1, ..a_m \rangle$ associated with the dipole. Here the cs and as are color indices, and the T matrices are $SU(3)$ matrices associated with the emitter and spectator

$$\frac{p \cdot \epsilon}{\lambda p \cdot q} \tag{3.8}$$

This turns out to be a universal factor for any parton emitting a soft gluon. The literature often refers to it as an eikonal factor [15] for soft gluon emission. If we note that for the full gluon emission process, any of the partons in the leading order process can emit a gluon, then this means that the full matrix element, in the soft limit $\mathcal{M}_{soft}$ looks like

$$\mathcal{M}_{soft} = \frac{4\pi\alpha_s}{\lambda} \sum_i \frac{p_i \cdot \epsilon}{q \cdot p_i} \mathcal{M}_{leadingorder} \tag{3.9}$$

Here the sum runs over all the initial and final state partons. The $4\pi\alpha_s$ comes from the two factors of the strong coupling that enter into the emission. Hence, the cross section, which goes like $\mathcal{M}^2$ approaches

$$|\mathcal{M}|^2_{soft} = \frac{1}{\lambda} \sum_{i,j} \frac{p_i \cdot p_j}{q \cdot p_i q \cdot p_j} |\mathcal{M}|^2_{LO} \tag{3.10}$$

Here we use the fact the polarization average of $p_i \cdot \epsilon p_j \cdot \epsilon = p_i \cdot p_j$. There are two collinear singularities wrapped up in this one expression (when q goes collinear with either p_j or p_i.) To separate them, we use

$$\frac{p_i \cdot p_j}{q \cdot p_i q \cdot p_j} = \frac{p_j p_i}{p_j \cdot q \, (p_i + p_j) \cdot q} + \frac{p_j p_i}{p_i \cdot q \, (p_i + p_j) \cdot q} \tag{3.11}$$

This is essentially just using partial fractions to decompose. So putting it all together , in the soft limit, the squared matrix element can be written

$$|\mathcal{M}|^2_{soft} = \sum_i \frac{1}{p_i \cdot q} \sum_{j \neq i} \frac{p_i \cdot p_j}{(p_i + p_j) \cdot q} |\mathcal{M}|^2_{LO} \tag{3.12}$$

From this term, we can understand the dipole terms. They depend on the leading order cross section, and a momentum dependent term. The momentum dependent term can be thought of as follows. An *emitter* parton i emits the gluon with momentum q, while a *spectator* parton j observes the emission.

While the term above smoothly approximates the NLO matrix element in the soft (and soft AND

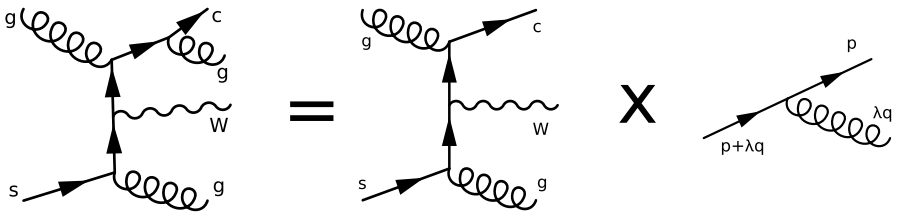

Figure 3.5: Dipole Factorization diagrammatically. In the collinear limit, the matrix element factorizes to the leading order multiplied by a dipole piece associated with collinear/soft divergences

collinear) region, it cannot be expected to correctly capture the behavior away from the soft limit. For this reason, we need to look at the behavior of the cross sections in the collinear limit.

In chapter 1, recall the DGLAP equation involved integrating over Alatarelli Parisi kernels. The piece that is divergent is exactly that part of the real matrix element that we remove via factorization, which means the collinear piece should be intimately related to the Altarelli Parisi kernel that showed up when we discussed collinear divergences before.

The first thing to do is to carefully define the collinear limit. If we have to two partons, p_i and p_j, with p_i an incoming parton, and p_j emitted off of p_i, we can define the collinear limit as follows[3]

$$p_j^\mu = (1-z)\, p_i^\mu + k_\perp^\mu - \frac{k_\perp^2\, n^\mu}{z 2p\cdot n} \tag{3.13}$$

Here, n is a null vector that we need to specify a perpendicular direction (k is perpendicular to both n and p_i). To see how this specifies a collinear direction, look at

$$2p_i \cdot p_j = -\frac{k_\perp^2}{(1-z)} \tag{3.14}$$

In the limit of $k_\perp \to 0$, these become our matrix element heads to the form

$$\mathcal{M}^2_{collinear} = \frac{4\pi\alpha_s}{z p_i p_j} P_{(ij),i}\,(z, k_\perp)\, \mathcal{M}^2_{LO} \tag{3.15}$$

Here the P is an Altarelli Parisi splitting kernel, just like we saw in the collinear limit before. Again, the $4\pi\alpha_s$ comes from the two factors of g^2. These kernels depend on the type of splitting (quark splitting

[3]We define the collinear limit slightly differently when we don't have an initial state parton. In particular, we need to define the collinear direction as well as the perpendicular direction

to quark and gluon, gluon splitting to gluons, etc).[4]

So the task of producing dipole subtraction terms amounts to the task of creating terms that, in the soft and collinear limit, reproduce the universal collinear and soft behaviors of the original NLO matrix elements. The squared matrix elements we will integrate for real corrections in the monte carlo program, then, look like

$$|\mathcal{M}|^2 = |\mathcal{M}|^2_{NLO,R} - \sum_{i,j,k} \mathcal{D}_{ij}^{ik,j} \, |\mathcal{M}|^2_{LO} \tag{3.16}$$

The terms $\mathcal{D}$ are called the dipoles, and the superscripts refer to parton i emitting parton k while parton j observes. The sum runs over all possible insertions of the extra gluon into the leading order matrix element. The dipoles should be chosen to match the momentum factor associated with soft emission,as well as the Alterelli Parisi kernel associated with the collinear divergences, for this reason there will be different dipoles for different emitting/emitter particles.

3.2.1 Building a Dipole

In what follows, I will give an example of one of these dipoles terms, demonstrate it has the right behavior in the soft and collinear limits, and then show that it is nicely analytically integrable so that we can add it to the virtual matrix elements.

For this specific calculation, we'll explore the an initial state quark i emitting a final state gluon k while a quark j watches. MCFM uses different dipole forms for final and initial partons because the phase space will factor differently depending on whether the emitter and observer partons are in the initial or final state [20, 21]. The dipole for this term looks like

$$\mathcal{D}_{qq}^{ik,j} = \frac{g^2 \mu^{2\epsilon}}{x p_i \cdot p_k} \left(\frac{2}{1-x} - 1 - x \right) \tag{3.17}$$

Here the superscripts represent the emitter/emitted and the observer. The subscripts represent emmiter/observer. The μ exists because we anticipate that when we integrate over the phase space later, we'll have a divergent integral. These divergences are handled analytically via dimensional regularization, where we work in in $4 - 2\epsilon$ dimensions to regularize the integral, and later take the $\epsilon \to 0$ limit. The subscripts

[4] The dependence on k that arises is to maintain spin/momentum correlations for gluon, quark emissions, we can have terms in the matrix element like $-f(z)\, g^{\mu\nu} + g(z)\, \frac{k_\perp^\mu \, k_\perp^\nu}{k_\perp^2}$.

indicates a quark emitting a quark. Above x is defined to be

$$x = 1 - \frac{s_{ik} + s_{jk}}{s_{ij}} \tag{3.18}$$

$$s_{ij} = (p_i + p_j)^2 = 2p_i \cdot p_j \tag{3.19}$$

In the soft limit emitted limit (small $|p_k|$), $x \to 1$, and $1 - x \to \frac{(p_i+p_j)\cdot p_k}{p_i \cdot p_j}$. Our dipole expression then becomes

$$\mathcal{D}_{qq}^{ik,j} \to \frac{g^2}{p_i p_k} \frac{2p_i \cdot p_j}{p_k \cdot (p_i + p_j)} \tag{3.20}$$

This exactly matches the soft momentum term associated with gluon emission discussed above, so our dipole certainly meats this criteria.

The next criterion is that it matches the relevant quark splitting function. For our case, the relevant splitting kernel is[5]

$$P_{qg} = \left(\frac{1 + x^2}{1 - x}\right) = \frac{2}{1 - x} - 1 - x \tag{3.21}$$

Now, in the collinear limit defined as before, we can note that $p_i \cdot p_k = 0$ and $p_j \cdot p_k = (1 - z)\, p_i \cdot p_j$. Hence,

$$x = 1 - \frac{s_{ik} + s_{jk}}{s_{ij}} = 1 - (1 - z) = z \tag{3.22}$$

So, we see that in the collinear limit, our, our dipole term becomes

$$\frac{g^2 \mu^{2\epsilon}}{x p_i \cdot p_k} \left(\frac{2}{1 - x} - 1 - x\right) = \frac{g^2}{z p_i \cdot p_k} \left(P_{qg}\left(z\right)\right) \tag{3.23}$$

So our dipole term also has the exact right behavior in the collinear limit. All that is left is to analytically integrate this so that it can be added back into a virtual matrix element. To do this integral, we will work

[5]This is without a color factor of $\frac{4}{3}$, because of the way MCFM handles dipoles

in $d = 4 - 2\epsilon$ dimensions and later take the limit of small epsilon. The original d dimensional, n particle phase space is

$$d^n\phi\left(p_i, p_j \to p_k, k_{n-1}\right) = \prod_{i=1,n} \frac{d^d p_i}{\left(2\pi\right)^{d-1}} \delta\left(p_i\right) \left(2\pi\right)^d \delta^d\left(p_i + p_j - \left(p_+ ...\right)\right) \tag{3.24}$$

To decompose the phase space, we note, we can break this up as follows

$$\int_0^1 dx d^{n-1}\phi\left(x p_i, p_j \to ...k_{n-1}\right) \left[dp_k\left(p_i, p_j, x\right)\right] \tag{3.25}$$

So we have to integrate the dipole over the term in square brackets. This term is

$$\left[dp_k\left(p_i, p_j, x\right)\right] = \frac{d^d p_k}{\left(2\pi\right)^{d-1}} \tag{3.26}$$

We change variables now to the variable x defined above, as well as $\nu = \frac{p_i \cdot p_k}{p_i \cdot p_j}$. Performing this change of variables leaves us with

$$\left[dp_k\left(p_i, p_j, x\right)\right] = \frac{\left(2p_i p_j\right)^{1-\epsilon}}{16\pi^2} \frac{d\Omega_{d-3}}{\left(2\pi\right)^{1-2\epsilon}} d\nu dx \theta\left(x\left(1-x\right)\right) \theta\left(\nu\right) \theta\left(1 - \frac{\nu}{1-x}\right) \left(1-x\right)^{-2\epsilon} \left[\frac{\nu}{1-x}\left(1 - \frac{\nu}{1-x}\right)\right]^{-\epsilon} \tag{3.27}$$

This, then is our phase space factor. $d\Omega_{d-3}$ is a solid angle factor perpendicular to the plane defined by p_i, and p_j.

The rest of the calculation involves performing the integrals and then expanding in powers of epsilon, discarding small terms. There is nothing particularly enlightening to be gained by fighting through the integral so, I will cut straight to the answer for our qq dipole.

$$\int \left[dp_k\left(p_i, p_j, x\right)\right] \left[x D_{qq}\right] = \left(\frac{\alpha_s}{2\pi}\right) \left[\left(\frac{1}{\epsilon^2} + \frac{1}{\epsilon}\left(\frac{3}{2} - L\right) + \frac{L^2}{2} - \frac{1}{2} - \frac{\pi^2}{6}\right) \delta\left(1-x\right)\right. \tag{3.28}$$

$$\left. + 1 - x - \frac{1+x^2}{1-x} \ln x - \left(1+x\right)\left(L + 2\ln\left(1-x\right)\right) + \frac{2L}{\left(1-x\right)_+} + 4\left[\frac{\ln\left(1-x\right)}{1-x}\right]_+\right] \tag{3.29}$$

Here, L is the log $\ln \frac{2p_i \cdot p_j}{\mu^2}$. This term can then be added back into the virtual matrix elements in order

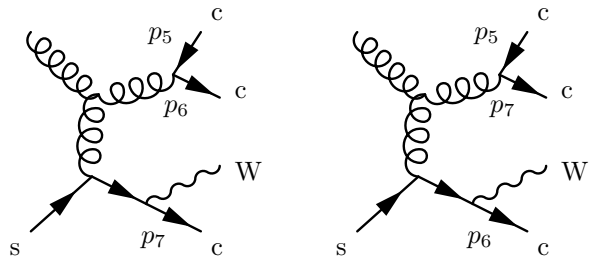

Figure 3.6: Two diagrams involved in $Wccc$ production

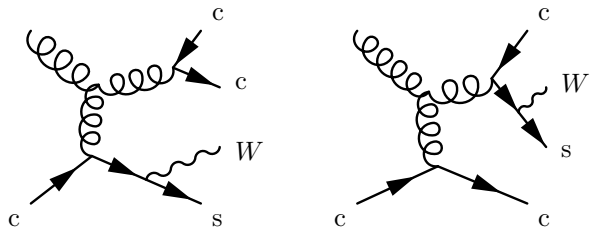

Figure 3.7: Two diagrams involved in $Wccj$ production

to obtain a finite integral.

3.3 The Need for Massive Quarks

There is yet another subtlety of this calculation. For everything so far we have assumed we can treat the charm quarks as massless. Unfortunately, this approximation cannot always be valid. Consider NLO correction where a final state gluon splits into a $c\bar{c}$ pair, shown in figure 3.6 and in the left side of figure 3.7.

If we consider the quarks as massive, the propagator for the gluon leading into the split takes the form (assuming the quarks are collinear)

$$\Delta \propto \frac{1}{k^2} = \frac{1}{p_1^2 + p_2^2 + 2p_1 \cdot p_2} = \frac{1}{2m_c^2 - 2E_c^2\,(1 - \cos\theta)} \tag{3.30}$$

After integrating, we expect the divergence to show up in the form

$$\ln \frac{E_c}{m_c} = \ln \frac{M_W}{m_c} \tag{3.31}$$

where M_W was picked as a representative scale for the process.

So for these processes, the collinear splitting is sensitive to the mass of the charm quark.

To simplify the calculation, we take only the charms involved in the splitting to be massive, this neglects interference between the two diagrams in figure 3.6. These interference effects are extremely small, only one of these diagrams can grow large in a given area of phase space. The left diagram grows large as p_5 and p_6 go collinear, while the right diagram grows large when p_5 and p_7 go collinear.

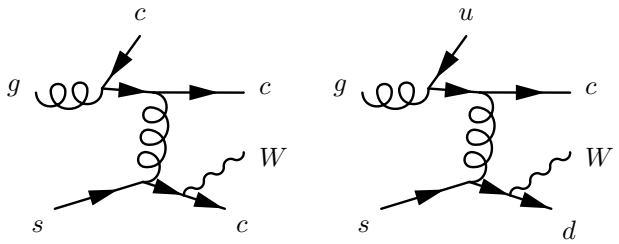

Figure 3.8: To maintain gauge invariance, the charm line at the top of both diagrams must be handled massively

A similar discussion applies to the diagrams in figure 3.7. Once again, we take only the collinear charm quarks in the left diagram as massive. This ignores interference terms between the two diagrams, but they are also small. [6]

The diagrams in 3.6 and 3.7 not only interfere with those of figure 3.8, they also have the same ordering of external legs, and are part of a gauge invariant set. To maintain gauge invariance, we have to consider the charm quark massive here as well. We won't use a dipole to cancel the massive logarithm that will show up from this divergence. Instead we'll need to cancel the initial divergence with a truncated charm distribution.

The physical insight is rather simple. When we integrate either diagram with the charm quark in the forward region, we'll get the usual logarithm of the mass, but this leading log term is already included in the heavy quark distribution function. To avoid over-counting, we need to subtract the log at this order in α_s from the charm distribution function.

$$\hat{c}\left(x,\mu_f\right) = \frac{\alpha_s}{2\pi}\ln\left(\frac{\mu^2}{m_c^2}\right)\int_x^1 \frac{dy}{y} P_{qg}\left(z\right) g\left(y\right) \tag{3.32}$$

Integrating this subtracted piece against the leading order diagram will cancel the mass logarithm associated with the initial state radiation in figure x above.

That takes care of the massive quarks in the real elements, but we have a similar final-state divergence in the virtual elements that we have to use a massive charm quark to regulate. The diagram shown in figure 3.9 has a final state divergence associated with the charm quark in the triangular loop.

The loop L has a denominator of the form

$$L \sim \frac{1}{k^2\left(k-p_1\right)^2\left(k-p_2\right)^2} = \frac{1}{k^2\left(k^2-2k\cdot p_1\right)\left(k^2-2k\cdot p_2\right)} \tag{3.33}$$

Now, when k goes collinear with p_2 (which implies $k^2 \sim 0$), $k\cdot p_2 \sim p_1\cdot p_2 > k^2$. So the denominator becomes

[6] To verify that these terms are small, we compared with a full calculation in MadGraph [22]with all three charms massive

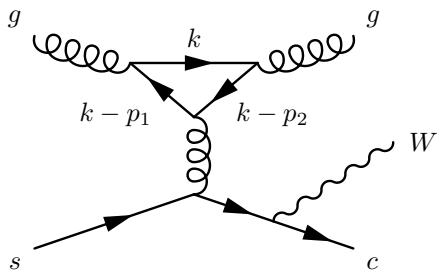

Figure 3.9: This virtual charm quark loop must be handled with non-zero mass or it has an uncanceled final state divergence.

$$L \sim \frac{1}{k^4 \left(-2p_1 \cdot p_2\right)} \tag{3.34}$$

This is logarithmically divergent, and this divergence is associated with the final state gluon.

For loops like that in figure 3.9 that do not involve charm quarks, this final stat collinear divergence would cancel against a divergence from the real splitting of the gluon to quarks in the real element. However, for charm quark loops we can't add this virtual process to a real splitting process because we can't combine processes with different numbers of final state charm quarks.

Just as we do for the final state divergence in the reals, we must regulate this with a finite charm mass. This process was not needed for the Wbj calculation, and was calculated specifically for this calculation. The full virtual process involves the triangle diagram in the figure, as well as quark bubbles on each of the gluons.

The diagram also has a collinear divergence associated with the initial state momentum of the gluon. In this case, we cancel the divergence by using a massive charm quark to regulate the divergence associated with virtual charm loops in the DGLAP kernel for P_{gg}, this results in the counter term in the equation below.[7]

$$\hat{\delta}\left(x, \mu_f\right) = \frac{\alpha_s}{2\pi} \ln\left(\frac{\mu_f^2}{m_c^2}\right) \frac{1}{3} g\left(x\right) \tag{3.35}$$

3.4 The Processes involved in the NLO calculation

Putting together everything in this chapter, the processes involved in the leading order calculation (both real and virtual corrections) can be seen in table 3.1

We can divide the output into several distinct processes. In the regions of phase space where we strictly

[7]This is analogous to equation 3.32. P_{gg} however, is more complicated than P_{qg}, having terms arising from real gg splitting, virtual gluon loops and fermion loops. Our counter term is exactly that part of P_{gg} that depends on the fermion loops.

$q\bar{q}' \to Wc\bar{c}$	one loop	$sq \to Wcq$	one loop
$sg \to Wcg$	one loop	$gc \to Wq'c$	one loop
$q\bar{q}' \to c\bar{s}W$	one loop	$gg \to c\bar{s}W$	one loop
$gs \to cgW$	one loop	$q\bar{q}' \to Wc\bar{c}g$	tree level
$sq \to Wcq'g$	tree level	$sg \to Wcgg$	tree level
$qc \to Wq'cg$	tree level	$q\bar{q} \to c\bar{s}Wg$	tree level
$gg \to c\bar{s}Wg$	tree level	$gs \to Wcgg$	tree level
$gq \to Wc\bar{c}q'$	tree level	$gq \to Wc\bar{s}q$	tree level
$gs \to Wc\bar{q}q$	tree level	$gc \to Wqc\bar{q}$	tree level

Table 3.1: All of the processes required for the NLO calculation. q or q' could be charm quarks. For instance $gs- > Wc\bar{q}q$ includes $gs \to Wc\bar{c}c$. For the tree level elements, we use the matrix elements of Nagy and Trocsanyi [1]. For the one loop elements, we use the matrix elements of Bern,Dixon and Kosower [2], with the exception being the massive charm loop where we instead use a finite charm quark mass to regulate the collinear divergence, which can be seen in the appendix.

produce two jets, we have exclusive production of Wcc or Wcj at NLO, depending on wether one or two jets is a charm. In these regions, we do NOT allow two charms to go collinear, each jet has either one, or no charms.

Wcc will still have contributions from those elements that contain 3 charms ($Wccc$) and Wcj will still have contributions from the real processes that produce two charms (Wcc) when one of the charms is very far forward. As discussed above, those in figure 3.8 are cancelled with massive quarks and a truncated charm distribution.

In regions where two charms go collinear, we have two charms in a single jet. We will call these processes $W(cc)j$ and $W(cc)c$. For these processes, we use massive charm quarks for the collinear pair, and neglect negligible interference terms as discussed above.

Chapter 4

Checks and Results

4.1 Checks

Before I present the results of the calculation, I first want to convince you that the calculation is actually correct.

Madgraph [22] can provide a powerful check on the tree-level elements, which have all been verified point-by-point in phase space against Madgraph's automatically generated code. MadDipole [23], an extension to madgraph, has provided the same check for the real dipole subtraction pieces.

In order to cross-check the virtual dipoles with the real dipoles, we used the alpha parameters suggested by Nagy and Trocsanyi [1]. Consider that a dipole generally has the form

$$\mathcal{D}_{ij,k} \propto \int_0^1 dz \frac{1}{z} P_{ij}(z) \tag{4.1}$$

where z is the parameter encoding the divergence (near $z = 0$).

Nagy and Trocsanyi suggested we only include the dipoles near a given divergence, so we can introduce a parameter α that ranges from near 0 to 1 and adjusts how much of the dipole to include.

$$\mathcal{D}_{ij,k} \propto \int_0^\alpha dz \frac{1}{z} P_{ij}(z) \tag{4.2}$$

This adds a non-trivial α dependence to the virtual and real dipoles. We can introduce a separate alpha parameter for initial-initial, initial-final,final-initial and final-final dipoles. Individually, both the real and virtual corrections will have α dependence, but the sum will not. This adds a strong check that the real and virtual terms contain the same dipoles.

A further check is that the Wcc calculation contains the Wbb calculation. By turning off the V_{cs} and V_{cd} elements we can turn off the exotic process in figure 2.2, in which case we have verified that we reproduce the Wbb result. Unfortunately, we cannot do the same thing for Wcj and Wbj since they depend on the initial charm and bottom pdfs, respectively.

The massive real elements are compared against a calculation done by madgraph in the region that the two quarks are collinear, which is the region where our approximation is valid. To check the virtual charm quark process, we compare the part that is finite in the limit $m_c \to 0$ with the massless virtual loops in Bern, Dixon and Kosower [2]. We also check that when both gluons are initial state gluons, that we can safely take the massless charm limit.

4.2 Results

The results for the NLO processes are shown in the tables and histograms below. Tables 4.1 contains the exclusive cross sections, and table 4.2 contains the inclusive cross sections and the uncertainties from varying renormalization,factorization and pdf uncertainties. As you can see from the tables, the corrections are rather modest, about 25%. More interesting, as can be seen in figures 4.1 and 4.2 the scale dependence is much weaker, so the overall scale uncertainty is substantially decreased. Below, I've produced a number of distributions at Tevatron and LHC parameters, and you can see that going to NLO does change the shape of the distributions a bit.

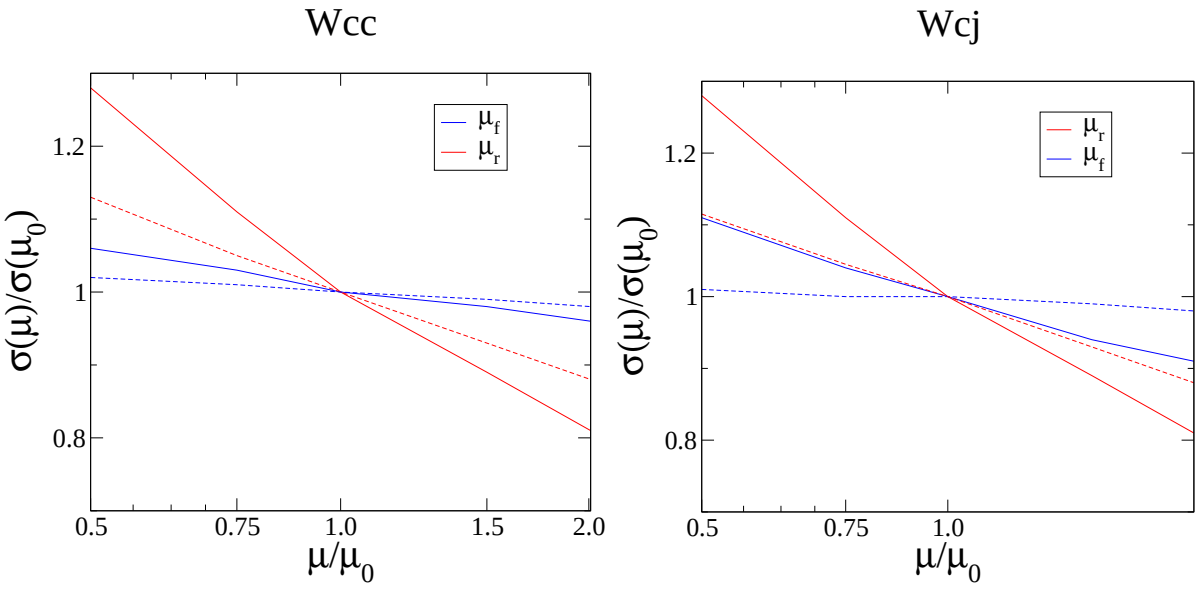

Figure 4.1: Scale dependence for Wcc and Wcj at LO and for inclusive NLO production at the Tevatron. The dashed line is NLO.

Table 4.1: Exclusive cross sections (pb) for W boson plus tw jets, with at least one c jet, at the Tevatron ($\sqrt{s} = 1.96$ TeV $p\bar{p}$, $p_T > 15$ GeV and $|\eta| < 2$) and LHC ($\sqrt{s} = 14$ TeV pp, $p_T > 25$ GeV and $|\eta| < 2.5$). Two final-state partons are merged into a single jet if $\Delta R_{jj} < 0.7$. No branching ratios or tagging efficiencies are included. The labels on the columns have the following meaning: Wcj = exactly two jets, one of which contains a c quark; $Wc\bar{c}$ = exactly two jets, both of which contain a c quark; $W(c\bar{c})j$ = exactly two jets, one of which contains two c quarks; $W(c\bar{c})c$ = exactly two jets, one of which contains two c quarks, the other a single c quark; $Wcjj$ = exactly three jets, one of which contains a c quark; $Wc\bar{c}j$ = exactly three jets, two of which contain a c quark;$Wccc$ = exactly three jets, all of which are c quarks. For the last set of processes, which include both light and heavy partons in the final state, the labels mean: Wjj = exactly two jets; $Wjjj$ = exactly three jets. For Wcj, $Wc\bar{c}$, and Wjj, both the leading-order (in parentheses) and next-to-leading-order cross sections are given. The CTEQ6M parton distribution functions are used throughout, except for the LO cross sections in parentheses, where CTEQ6L1 is used [3]. The factorization and renormalization scales are chosen as $\mu_F = \mu_R = M_W$.

	Cross sections (pb)						
Collider	Wcj	$Wc\bar{c}$	$W(c\bar{c})j$	$W(c\bar{c})c$	$Wcjj$	$Wc\bar{c}j$	$Wc\bar{c}c$
TeV $W^+(=W^-)$	(15.8)19.9	(2.56)3.10	2.85	0.10	2.64	0.64	0.012
LHC W^+	(672)528	(17.4)21.8	57.4	6.29	169	13.1	0.873
LHC W^-	(695)533	(15.5)18.0	39.2	7.01	175	9.54	0.999
	Wjj				$Wjjj$		
TeV $W^+(=W^-)$	(261) 290				39		
LHC W^+	(4990) 4170				1280		
LHC W^-	(3650) 3030				890		

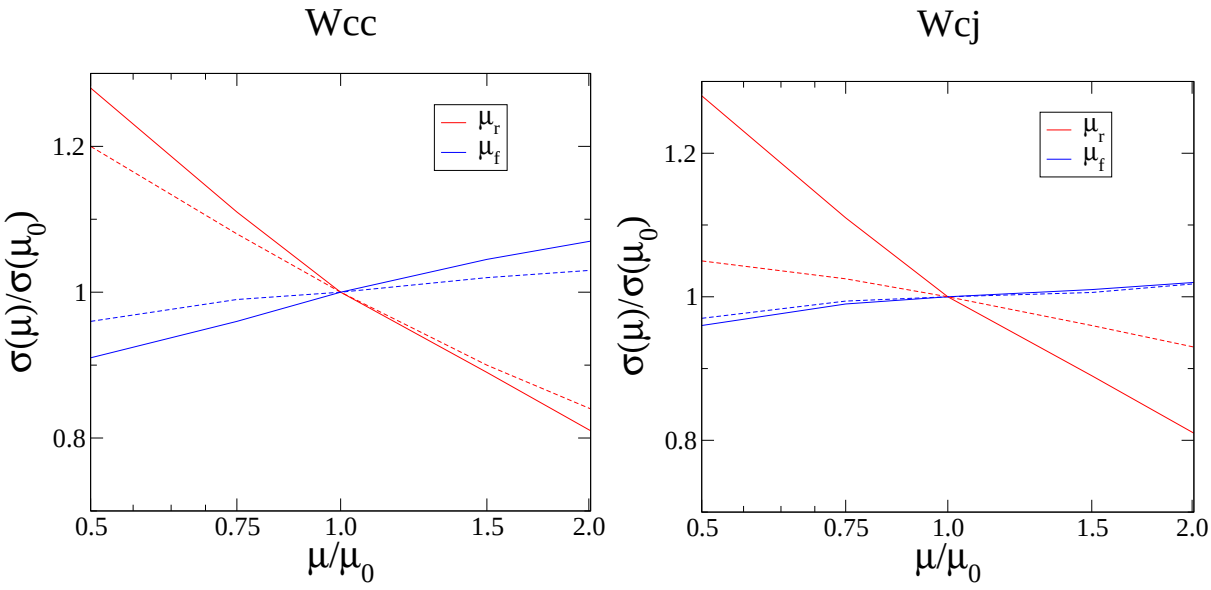

Figure 4.2: Scale dependence for Wcc and Wcj at LO and for inclusive NLO production at the LHC. The dashed line is NLO

Table 4.2: Inclusive cross sections (pb) for W boson plus two (or more) jets, with at least one c jet, at the Tevatron ($\sqrt{s} = 1.96$ TeV $p\bar{p}$, $p_T > 15$ GeV and $|\eta| < 2$) and LHC ($\sqrt{s} = 14$ TeV pp, $p_T > 25$ GeV and $|\eta| < 2.5$). Two final-state partons are merged into a single jet if $\Delta R_{jj} < 0.7$. No branching ratios or tagging efficiencies are included. The labels on the columns have the following meaning: $Wcj + X$ = two or more jets, one of which contains a c quark; $Wc\bar{c} + X$ = two or more jets, both of which contain a c quark; $W(c\bar{c})j$ = exactly two jets, one of which contains two c quarks; $W(c\bar{c})c$ = exactly two jets, one of which contains two c quarks, the other a single c quark; For the last set of processes, which include both light and heavy partons in the final state, the labels mean: $Wjj + X$ = two or more jets; For $Wcj + X$, $Wc\bar{c} + X$, and $Wjj + X$, both the leading-order (in parentheses) and next-to-leading-order cross sections are given. The CTEQ6M parton distribution functions are used throughout, except for the LO cross sections in parentheses, where CTEQ6L1 is used [3]. The factorization and renormalization scales are chosen as $\mu_F = \mu_R = M_W$. The uncertainties are from the variation of the renormalization scale, the factorization scale, and the parton distribution functions, respectively.

	Cross sections (pb)			
Collider	$Wcj + X$	$Wc\bar{c} + X$	$W(c\bar{c})j$	$W(c\bar{c})c$
TeV $W^+(= W^-)$	$(15.8)22.5^{+2.6\,+0.2\,+1.3}_{-2.6\,-0.4\,-1.3}$	$(2.56)3.74^{+0.48\,+0.08\,+0.12}_{-0.44\,-0.07\,-0.12}$	$2.85^{+1.15\,+0.26\,+0.09}_{-0.75\,-0.23\,-0.09}$	$0.10^{+0.08\,+0.04\,+0.01}_{-0.02\,-0.01\,-0.01}$
LHC W^+	$(672)697^{+34\,+19\,+36}_{-49\,-18\,-36}$	$(17.4)35.0^{+7.0\,+1.1\,+1.2}_{-5.6\,-1.5\,-1.2}$	$57.4^{+23.2\,+0.3\,+2.1}_{-15.0\,-1.3\,-2.1}$	$6.29^{+2.56\,+0.15\,+0.2}_{-1.64\,-0.22\,-0.2}$
LHC W^-	$(695)708^{+22\,+9\,\,+35}_{-51\,-18\,-35}$	$(15.5)27.5^{+5.0\,+1.5\,+0.9}_{-3.8\,-1.5\,-0.9}$	$39.2^{+15.9\,+0.5\,+1.0}_{-10.2\,-0.9\,-1.0}$	$7.01^{+2.81\,+0.11\,+0.2}_{-1.85\,-0.22\,-0.2}$
	$Wjj + X$			
TeV $W^+(= W^-)$	$(261)\ 329^{+30\ +6\ +7}_{-32\ -6\ -7}$			
LHC W^+	$(4990)\ 5450^{+410\ +70\ +190}_{-480\ -0\ \ -190}$			
LHC W^-	$(3650)\ 3920^{+300\ +60\ +150}_{-310\ -10\ -150}$			

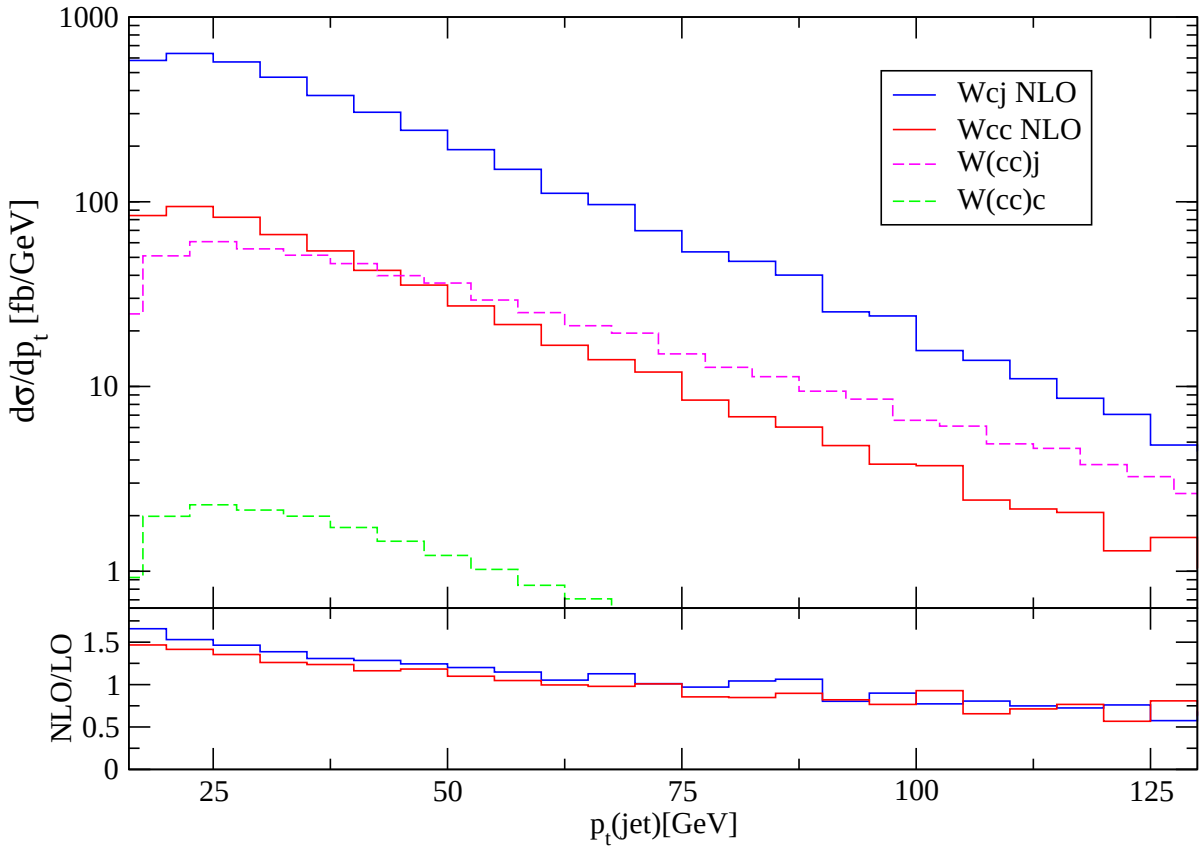

Figure 4.3: Exclusive cross section for Wcj and Wcc at NLO at the Tevatron vs the p_t of the highest jet. The dashed lines are the processes for $W(cc)j$ and $W(cc)c$. The lower plot contains the ratio of the NLO to LO cross sections. All parameters as described for TeV in table 4.1

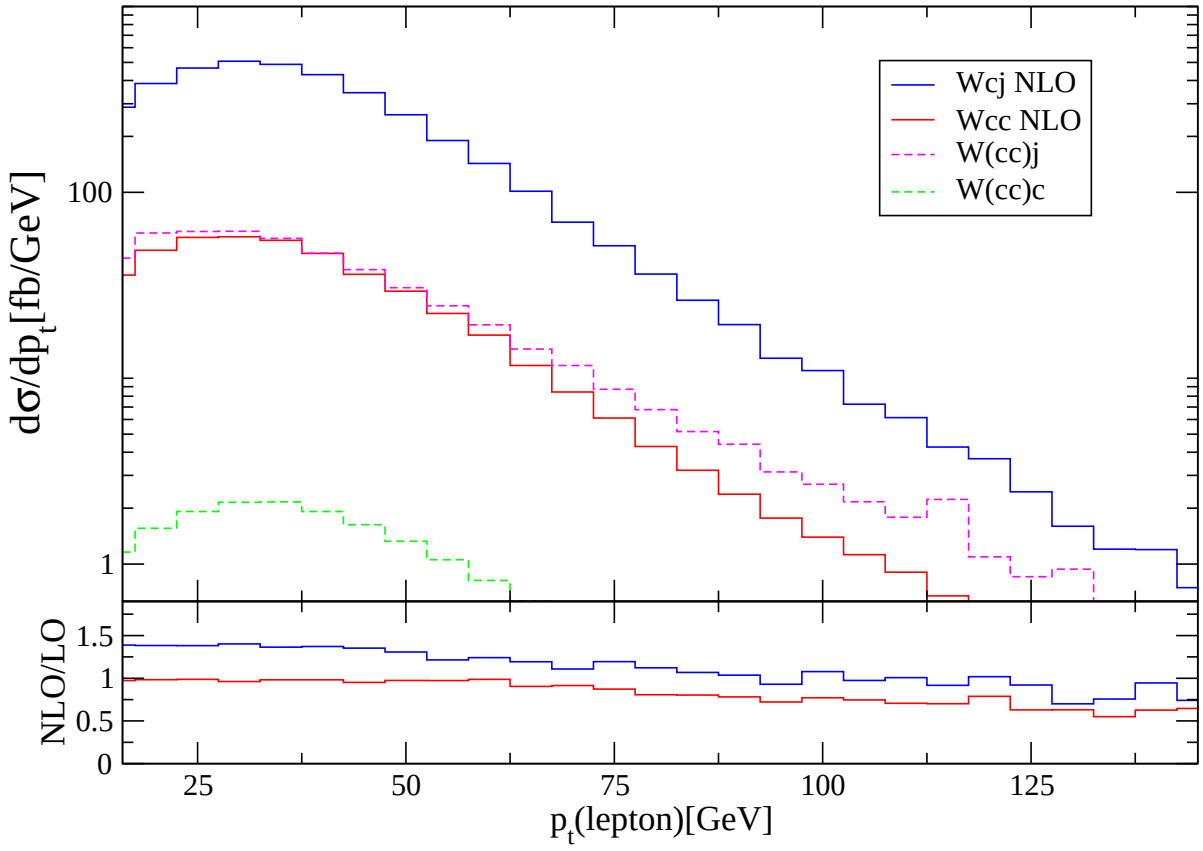

Figure 4.4: Same as figure 4.3 but for the p_t of the lepton from W decay

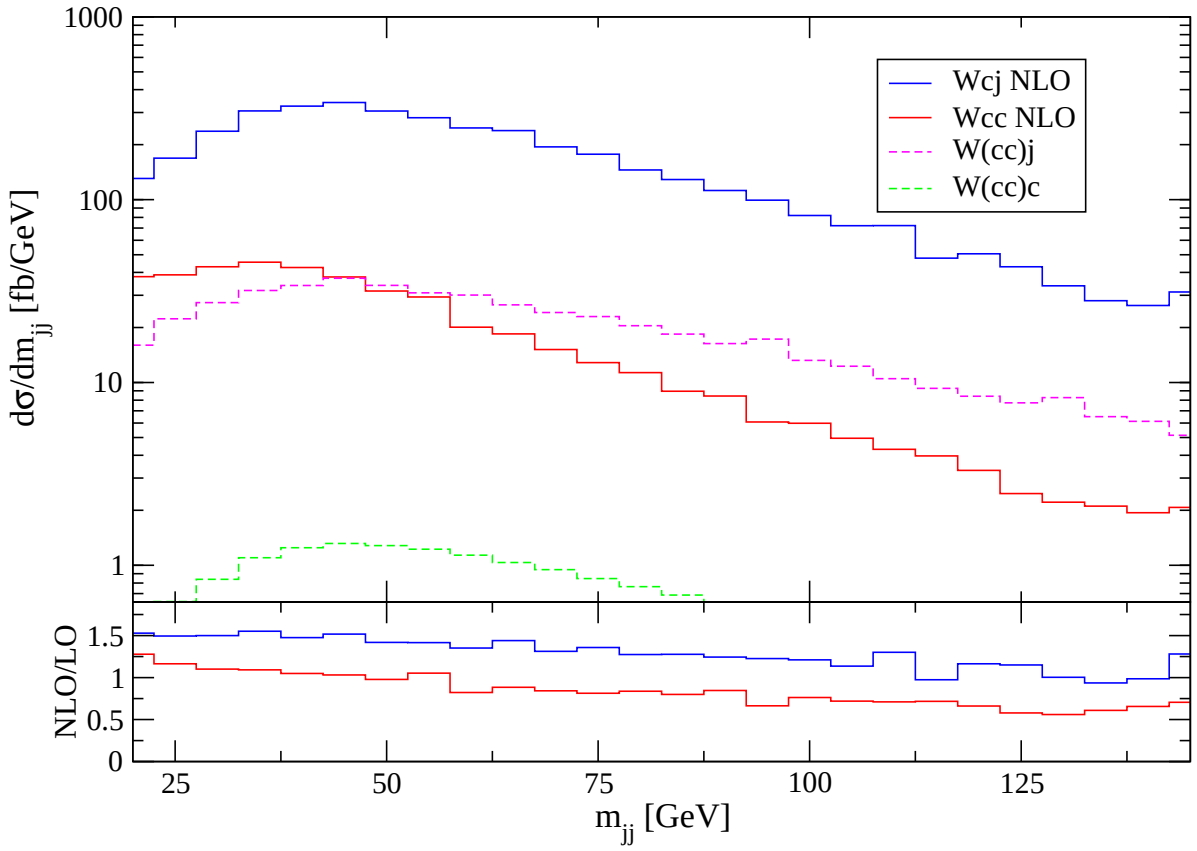

Figure 4.5: Same as figure 4.3 but for the dijet invariant mass

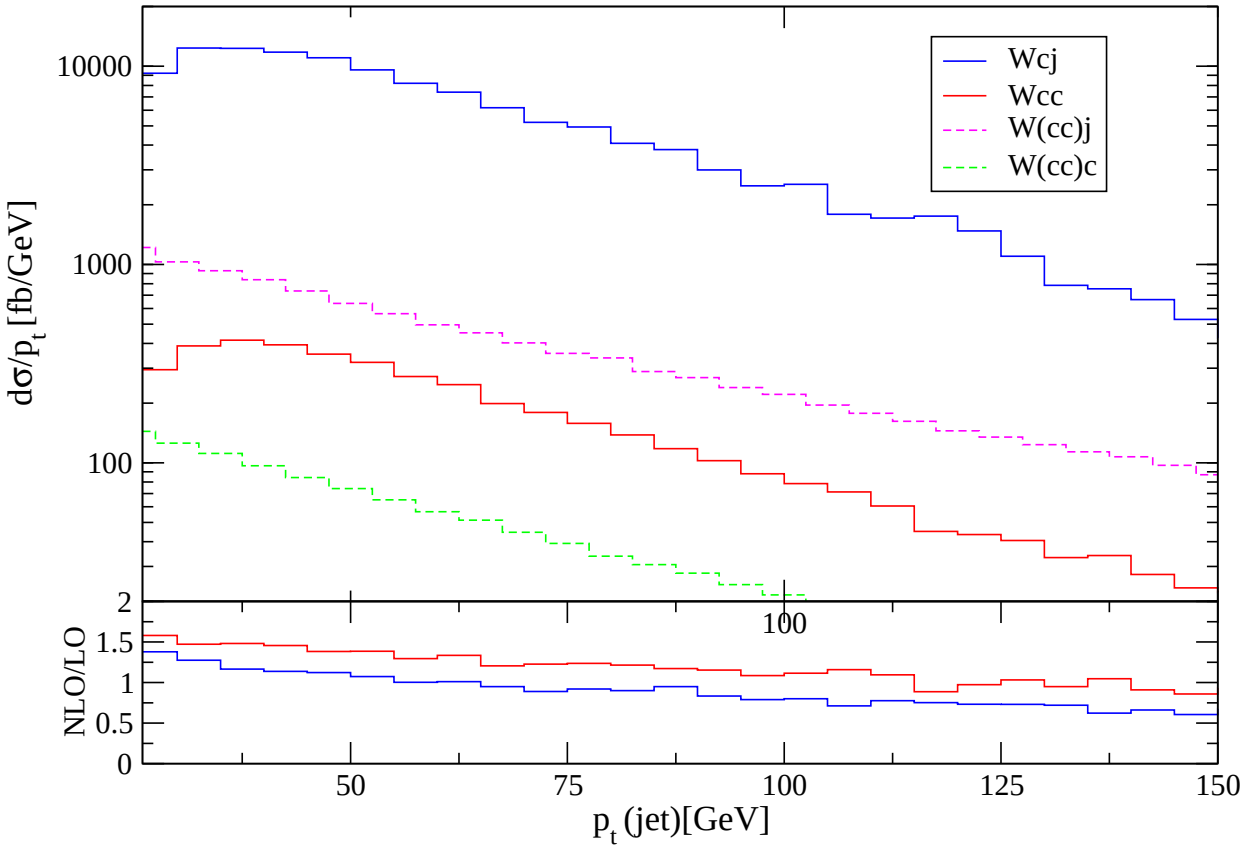

Figure 4.6: Exclusive cross section for Wcj and Wcc at NLO at the LHC vs the p_t of the highest jet. The dashed lines are the processes for $W(cc)j$ and $W(cc)c$. The lower plot contains the ratio of the NLO to LO cross sections. All parameters as described for LHC in table 4.1

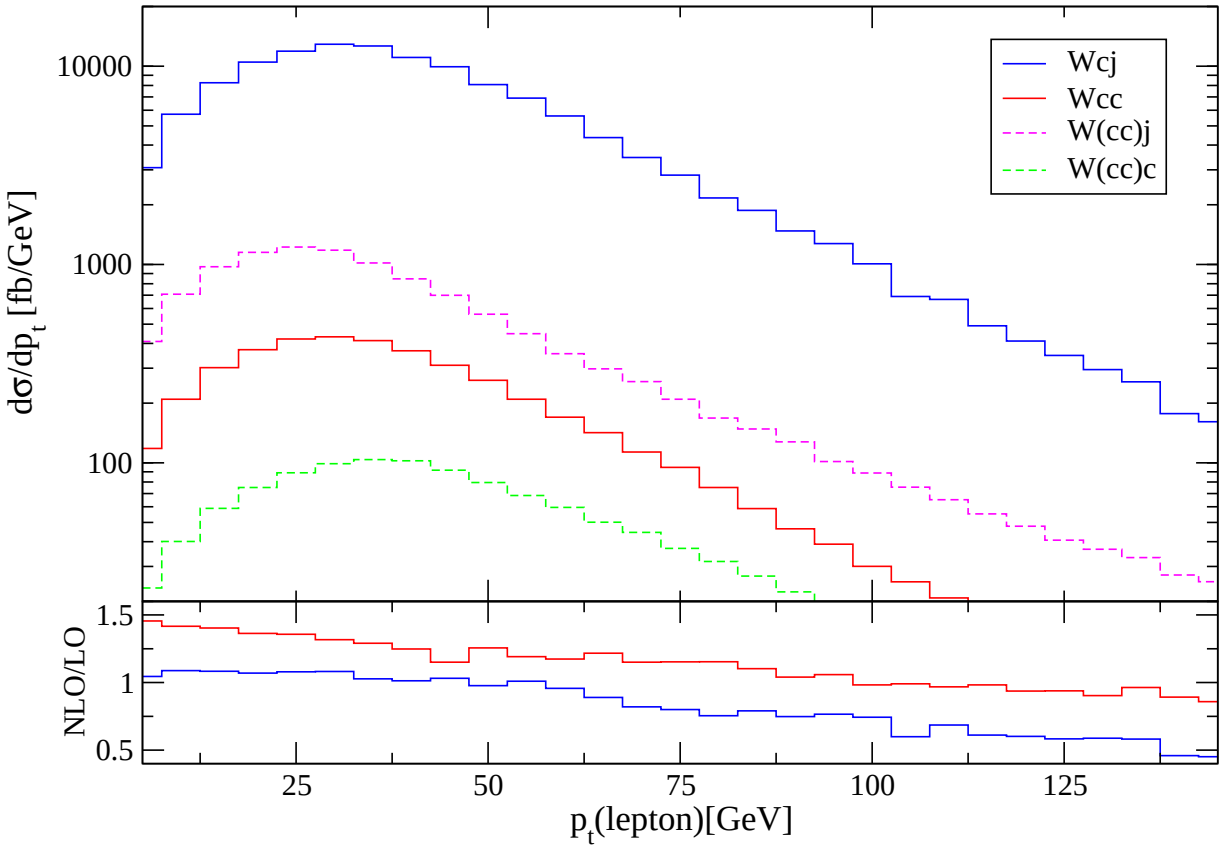

Figure 4.7: Same as figure 4.6 but for the p_t of the lepton from W decay

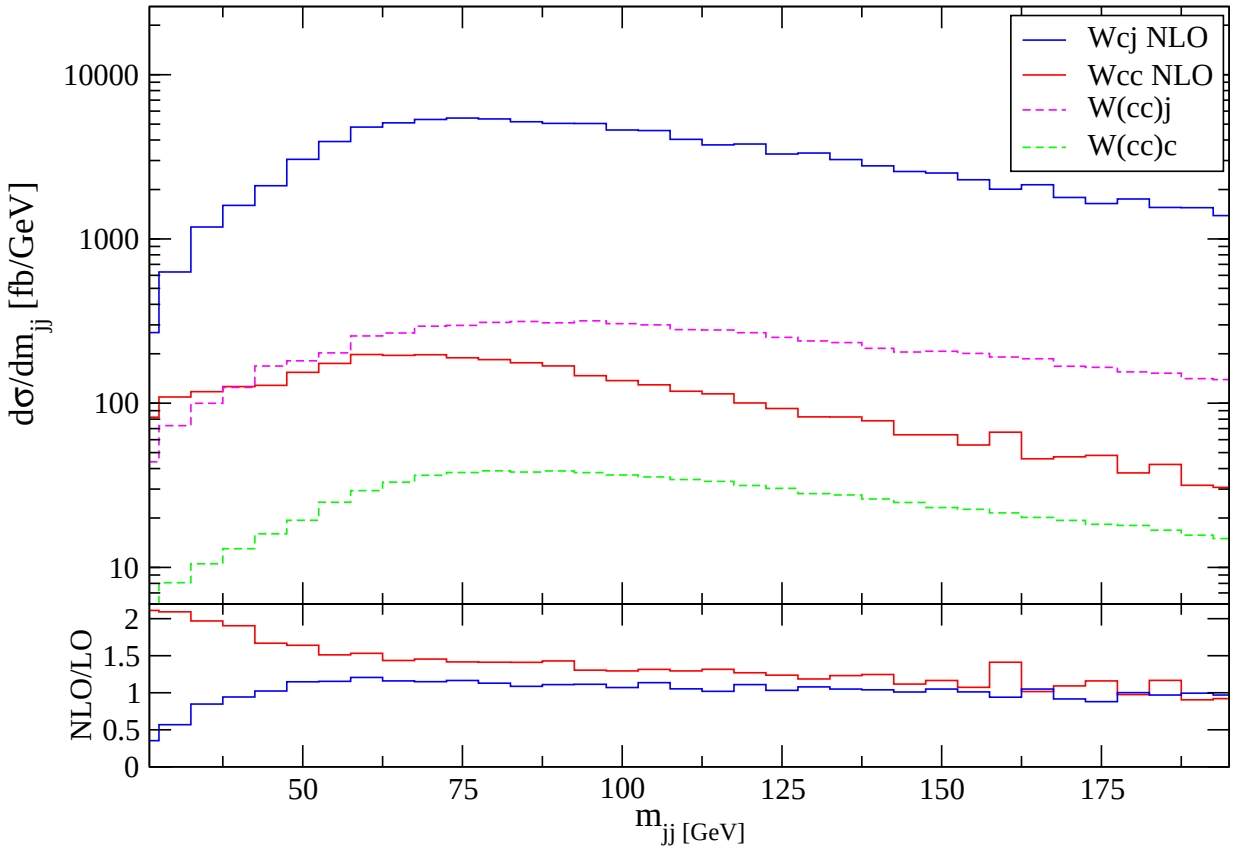

Figure 4.8: Same as figure 4.6 but for the dijet invariant mass

Appendix

The Massive Loop Matrix Element

Following the notation of Bern, Dixon and Kosower (BDK), we note that we can separate the amplitude into a few partial amplitudes. These are defined by color-ordered Feynman rules and are individually gauge invariant. Using their notation, and with the CKM element of the quark suppressed.

$$\begin{aligned} A_6^{1-\text{loop}}\left(1_q,2,3,4_{\bar{Q}}\right) = 2e^2g^4\mathcal{P}_W\left(s_{56}\right)\Bigg[N_c\sum_{\sigma\in S_2}\left(T^{a\sigma(2)}T^{a\sigma(3)}\right)_{i_1}^{\bar{i}_4}A_{6;1}\left(1_q,\sigma\left(2\right),\sigma\left(3\right),4_{\bar{Q}}\right) \\ +\delta^{a_2,a_3}\delta_{i_1}^{\bar{i}_4}A_{6;3}\left(1_q,4_{\bar{Q}},2,3\right)\Bigg] \end{aligned} \tag{.1}$$

This suppresses dependence on 5 and 6 which are the charged lepton and neutrino associated with the W boson. The second term can't have a charm-quark loop of the type in figure 3.9, because charge-conjugation invariance/Furry's theorem implies that the the partial amplitudes have to be anti-symmetric in momenta 2 and 3, so the color structure must also be anti-symmetric to have a non-zero amplitude.

We can further decompose $A_{6;1}$ a piece proportional to the number of fermions n_f, and pieces that are not.

$$A_{6;1}\left(1_q,2,3,4_{\bar{Q}}\right) = A_6\left(1_q,2,3,4_{\bar{Q}}\right) - \frac{1}{N_c^2}A_6\left(1_q,4_{\bar{Q}},3,2\right) - \frac{n_f}{N_c}A_6^f\left(1_q,2,3,4_{\bar{Q}}\right) \tag{.2}$$

Because the piece proportional the number of fermions has to be independently gauge invariant, we can treat it separately.

Doing the loop with non-zero charm mass, holding only terms divergent in the charm mass we find (note, all momenta are outgoing, in keeping with BDK),

$$\begin{aligned} A_6^f\left(1_q^+,2^+,3^+,4_{\bar{Q}}^-\right) = i\left(\frac{1}{\left(4\pi\right)^{2-\epsilon}}\frac{\Gamma\left(1+\epsilon\right)\Gamma^2\left(1-\epsilon\right)}{\Gamma\left(1-2\epsilon\right)}\right)\Bigg[\left(\frac{2}{3\epsilon}-\frac{2}{3}\ln\left(\frac{s_{23}}{m_c^2}\right)\right)\frac{-\left\langle 45\right\rangle^2}{\left\langle 12\right\rangle\left\langle 23\right\rangle\left\langle 34\right\rangle\left\langle 56\right\rangle} \\ +\frac{1}{3\left\langle 23\right\rangle}\left(-\frac{\left\langle 45\right\rangle\left[6\right|\left(1+2\right)3\left|1\right]}{t_{123}}+\frac{\left[16\right]\left\langle 5\right|\left(4+2\right)3\left|4\right\rangle}{t_{234}}\right)\Bigg] \end{aligned} \tag{.3}$$

The notation here is the same as BDK, $\langle n| = \langle k_n^-|$, $[n| = \langle k_n^+|$, $|n\rangle = |k_n^+\rangle$, $|n] = |k_n^-\rangle$, and $\langle l|\, mn...\, |o\rangle = \langle k_l^- | \not{k}_m \not{k}_n ... |k_o^+\rangle$, etc. k is the particle 4-momentum.

Also, $s_{ij} = 2p_i \cdot p_j$ and $t_{ijk} = (k_i + k_j + k_l)^2$.

The uncanceled ϵ is an ultraviolet divergence that cancels against part of the $\overline{MS}$ subtraction term:

$$g^2 N_c \left(\frac{1}{(4\pi)^{2-\epsilon}} \frac{\Gamma(1+\epsilon)\,\Gamma^2(1-\epsilon)}{\Gamma(1-2\epsilon)} \right) \left[\frac{1}{\epsilon} \left(\frac{11}{3} - \frac{2}{3} \frac{n_f}{N_c} \right) \right] A_6^{LO} \tag{.4}$$

References

[1] Z. Nagy and Z. Trocsanyi, Phys. Rev. **D59**, 014020 (1999).

[2] Z. Bern, L. J. Dixon, and D. A. Kosower, Nucl. Phys. **B513**, 3 (1998).

[3] J. Pumplin *et al.*, JHEP **07**, 012 (2002).

[4] S. S. D. Willenbrock and D. A. Dicus, Phys. Rev. **D34**, 155 (1986).

[5] T. Stelzer, Z. Sullivan, and S. Willenbrock, Phys. Rev. **D56**, 5919 (1997).

[6] J. Campbell, R. K. Ellis, F. Maltoni, and S. Willenbrock, Phys. Rev. **D75**, 054015 (2007).

[7] D. E. Acosta *et al.*, Phys. Rev. **D71**, 012005 (2005).

[8] V. M. Abazov *et al.*, Phys. Lett. **B622**, 265 (2005).

[9] D. E. Acosta *et al.*, Phys. Rev. Lett. **95**, 051801 (2005).

[10] V. M. Abazov *et al.*, Phys. Rev. Lett. **94**, 091802 (2005).

[11] M. Peskin and D. Schroeder, *An Introduction to Quantum Field Theory* (Westview Press, ADDRESS, 1995).

[12] K. Wilson and J. Kogut, Physics Reports **12**, 75 (1974).

[13] S. Willenbock, Summer School Lectures (1989).

[14] R. Feynman, (1972).

[15] R. Ellis, W. Stiring, and B. Webber, *QCD and Collider Physics* (Cambridge University Press, ADDRESS, 1996).

[16] J. Campbell and R. K. Ellis, mcfm.fnal.gov (2007).

[17] T. Kinoshita, J. Math. Phys. **3**, 650 (1962).

[18] T. D. Lee and M. Nauenberg, Phys. Rev. **133**, B1549 (1964).

[19] J. Collins, D. Soper, and G. Sterman, Perturbative quantum chromodynamics 1 (1989).

[20] S. Catani and M. Seymour, Nuclear Physics B **485**, 291 (1997).

[21] J. M. Campbell and R. K. Ellis, Phys. Rev. **D62**, 114012 (2000).

[22] F. Maltoni and T. Stelzer, JHEP **02**, 027 (2003).

[23] R. Frederix, T. Gehrmann, and N. Greiner, Journal of High Energy Physics **2008**, 122 (2008).